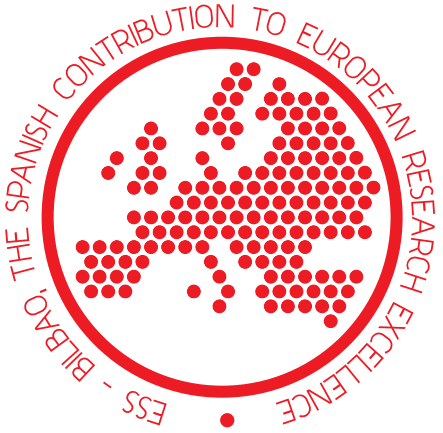

DESIGN REPORT: Target Vessel

Reference:	ESS-0109614
Date:	June 5, 2019
Revision:	2.0

Author	**Review**	**Approved**
F. Sordo	R. Vivanco	F. Sordo

List of contributors: J. Aguilar, A. Aguilar, O. Gonzalez, R. Vivanco, M. Magan, P. Luna, S. Stepanyan, F. J. Villacorta.

Contents

1 Introduction

Neutron spallation sources are devices designed to produce neutrons from spallation nuclear reactions. In order to produce this kind of reactions it is necessary to accelerate protons (H+ particles) using electromagnetic fields up to they get a huge amount of kinetic energy or speed close to light velocity. In that moment, protons are led to impact on a nucleus of a heavy atom (generally mercury, lead or tungsten) producing what it is known as spallation reaction.

The place where the reaction is produced it is known as spallation Target and it is considered the neutron source. This Targets are complex devices, from an engineering point of view, where a huge amount of heat is deposited on the spallation material. In some cases, it is note that the heat density in the spallation target can be higher than fuel bars inside a nuclear power reactor, as a consequence the design of spallation Target is a real engineering challenge. The ESS target is one of these cases.

The European spallation Source (ESS) is an ambitious European project with a budget higher to 1.800 M€. The aim of the project is to design, build and operate the most important and the bright spallation neutron source in the world. The ESS will use a proton beam with final power deposited on the target of 5.2 MW (five times higher than SNS and JPARC), which will impact on a tungsten Target cooled by helium gas.

The Target will be designed with a set of tungsten blocks placed inside of a wheel of $\sim$ 2.6 meter of diameter. Protons will impact at high speed on the wheel in a radial direction. Inside the wheel, helium flows at high velocity, cooling the tungsten blocks dissipating the heat produced by the nuclear reactions. The wheel rotates at a speed of 0.2-0.5 Hz, so the proton beam impacts on a different region of the wheel at a repetition rate of 14 Hz, distributing the heat over the whole perimeter of the wheel.

The aim of this document is to describe the following aspects that justify the technical decisions associated to the design of the Target Vessel:

- Loads and requirements
- Radiation damage conditions
- Thermomechanical conditions on normal operations (SF1)
- Thermomechanical conditons on accidental cases (SF2, SF3 and SF4)

The Target Vessel is not a Safety related component according ESS definition[1]. However, is one of the critical elements for the operation of the facility and so, in order to have a high quality equipment, the $RCC-MR_x$ design rules should be applied to the component for $N2R_x$ level.

2 Load scenarios

The operational conditions that the component have to withstand along its life time are defined as "load scenarios". The load scenarios are classified based on SF levels[3]:

- SF 1 and 2 are operating conditions associated with Normal operation, start and stop, and normal operational incidents.
- SF 3 Conditions are Operating Conditions which are rare and leads to shutdown and inspection, limit to 10 times in the lifetime.
- SF 4 Conditions are highly improbable but relevant for safety.

Based on the inspection conditions and actions after the scenario, a protection level is associated with the component (Level A, C or D). According to activation levels of the equipment, inspection after the accidental event is not possible hence, events are classified on Levels A (restart is possible after the event) or D (restart is not possible after the event).

Regarding the different operational scenarios [1], Tables 1 and 2 shows the events considered for the target vessel design and its protection level.

Table 1 shows several accidental cases in which the engineering solution for the Target Vessel will no play a significant role for the behaviors of the system. These load conditions will be evaluated on safety analysis documents [2], but they are not in the scope of this document. The following load cases will not be considered:

- Global bypass: The internal bypass in the vessel is difficult to describe due to the different casuistic. However, in all of them the vessel will be partially cooled hence, temperature evolution will be lower that the scenarios associated to mass flow reduction. Hence, the evaluation of mass flow reduction cover this scenario.

Requirement		**Loads[1]**	**Level**	**Prot.**
Design Conditions	B02	Design pressure (13 bar(g)) Design Temperature (500^oC)	SF1	A
Nominal Conditions	B01	Design Beam [5] Operating pressure (12 bar(g)) Operational cooling conditions (2.85 kg s^{-1}) Wheel rotation	SF1	A
Vertical displa.	B10	Design Beam [5] displaced 10 mm Operating pressure (12 bar(g)) Operational cooling conditions (2.85 kg s^{-1}) Wheel rotation	SF2	A
Desynchronization	B09	Design Beam [5] on rib Operating pressure (12 bar(g)) Operational cooling conditions (2.85 kg s^{-1}) Wheel rotation	SF2	A
Shut-down	B08	No beam No coolant flow Wheel stopped	SF2	A
Loss of coolant	B06	Nominal beam Operating pressure (12 bar) Operational cooling conditions ($<$ 2.85 kg s^{-1}) Wheel rotation	SF2	A
Global bypass*	B06	Nominal beam Operating pressure (12 bar) Operational cooling conditions (2.85 kg s^{-1}) Internal bypass Wheel rotation	SF2	A

Table 1: Operational Scenarios identified for the Target Vessel[4]

Requirement		Loads[1]	Level	Prot.
Raster focused beam	B05	raster focused Beam [5] Operating pressure (12 bar(g)) Operational cooling conditions (2.85 kg s^{-1}) Wheel rotation	SF3	A
Undrastered beam	B04	Raster failure Beam [5] Operating pressure (12 bar(g)) Operational cooling conditions (2.85 kg s^{-1}) Wheel rotation	SF3	A
Stopped wheel	B03	Nominal Beam [5] Operating pressure (12 bar(g)) Operational cooling conditions (2.85 kg s^{-1}) Wheel stopped	SF4	D
Unrastered-overfocused beam		Focused non raster Beam [5] Operating pressure (12 bar(g)) Operational cooling conditions (2.85 kg s^{-1}) Wheel rotation	SF4	D

Table 2: Operational Scenarios identified for the Target Vessel[4]

3 ESS Target configuration

The configuration of a 5.2 MW spallation target is a complex process and there is no an unique solution. Also it should be remark that most of the activated material produced in the spallation reactions will be confine in the target. For that reason the target design is close related to ESS safety issues. In order to guide the selection of the target concept, ESS organized a working group in order to explore several Target options (Target Selection Concept Phase, TSCP). This working group explored several target options from 2010 to 2012, [2].

After this process, ESS selected as final solution a solid rotating target cooled by helium. This solution was developed further by ESS and KIT along 2012-2013 and its final concept is summarized on the TDR proposal.

On November 2014, ESS-Bilbao was choose as in-kind partner for Target Wheel, shaft and drive unit. The redesign works started on January 2015. Along this period, ESS-Bilbao has follow and optimization process summarized on the Report [11] that arrives to a new base line proposal in June 2015. The previous configurations analysis is not in the scope of this document.

The proposed new target configuration is based on 10x30x80 mm^3 tungsten bricks. These tungsten bricks are placed on an steel support (the cassette), in a cross flow configuration as it is shown on Figure 1.

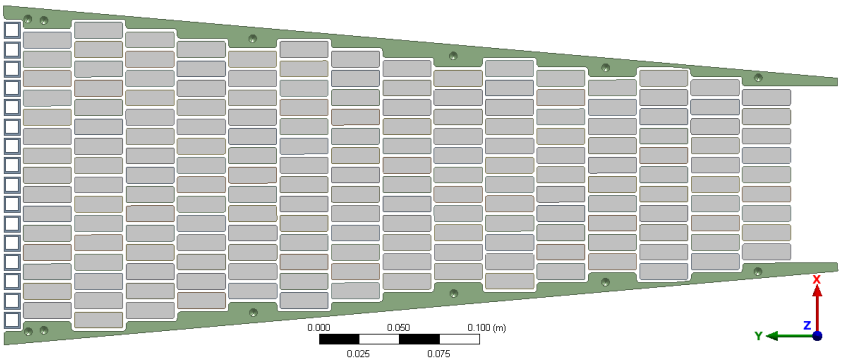

Figure 1: Tungsten bricks(grey) and turbulence generators final (blue) configuration on a Target Wheel sector.

The cassette withstand tungsten bricks and configures the let helium channels in the gap between ribs and target vessel (Figure 1). Finally, 36 of these cassettes will be assembled in a sectored wheel as it is shown on Figure 2.

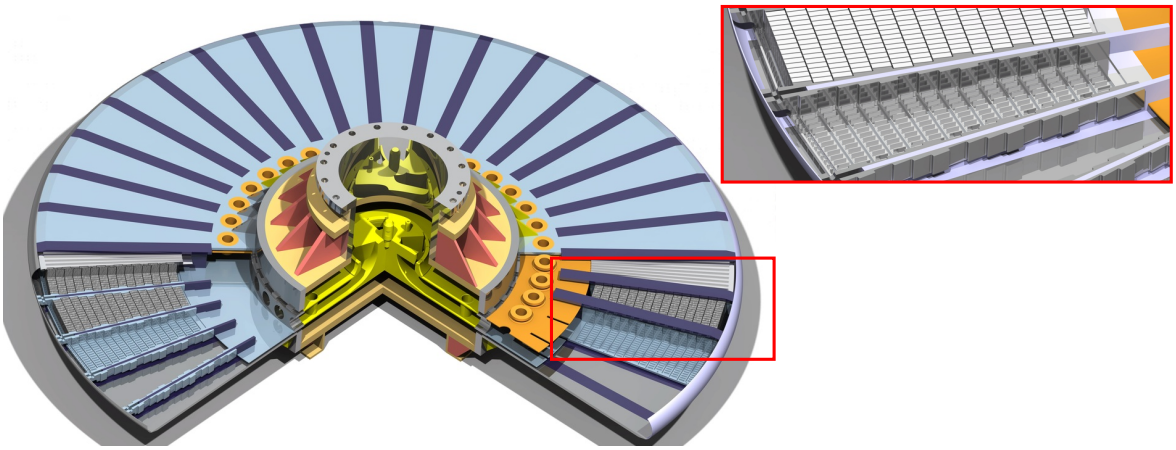

Figure 2: Target wheel configuration

The external surface of the assembled wheel that constitutes the pressure barrier is the Target Vessel (Figure 3). The TV is composed by two 11 mm disk (2 and 3) joint by vertical ribs (4). The inner diameter of the disks is welded to a forge ring that in with 108 inlet/oulet holes for cooling are machined (1) and they include cilindrical holes to introduce temperature mesurement

system (described on [7]). Finally the geometry is closed by the proton beam window (5). As it is described in the manufacturing plan[34] all the sections of the TV are welded by TIG.

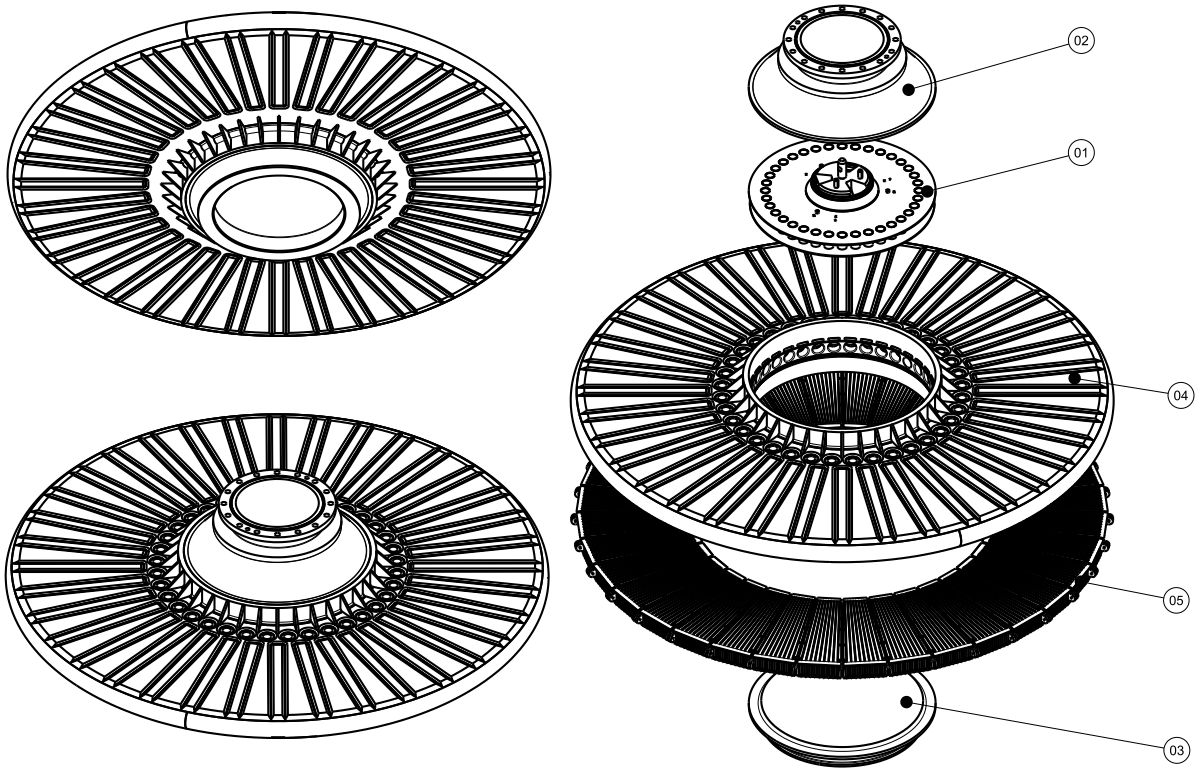

Figure 3: Target Vessel geometry

4 Materials properties and operational limits

The ESS Target Vessel Wheel, will be manufactured on austenitic Stainless Steel (SS-316L). This alloy its frequently used on nuclear industry due to is good corrosion resistance properties and moderate radiation resistance. Also, this alloy can be welded with standard TIG/MIG techniques, even in thickness above 10 cm with very high quality. Finally, due to its frequent use on non-nuclear industry all the manufacturing technologies required for this material are widely available.

Mechanical properties for lineal model analysis have been taken from ESS Material's Handbook[9], which is completely consistent with $RCC - MR_x$ Appendix A[3].

Based on the scenario under analysis, the device has to be protected against different types of damage. This protection criteria are categorized in several levels. The nominal conditions (SF1,SF2) analyzed in this report are included in the Level A. Accidental conditions (SF3) are included on Level D.

Tables 3 and 4 show the Mechanical Stress limits for primary and secondary loads for both protection levels.

Temp (^oC)	**100**	150	**200**	250	300
S_m (MPa)	127	127	123	114	106
S (MPa)	119	114	108	106	106
$R^t_{p0.2}min$ (MPa)	165	150	137	127	118
(R_m)min (MPa)	430	–	390	–	380
$\underline{Peak}$					
1.5 * $S_m = S^A_m$ (MPa)	190.5	190.5	184.5	171	159
$\underline{Welding}$					
S_m * 0.85 (MPa)	107.95	107.95	104.55	96.9	90.1
S_m * 0.70 (MPa)	88.9	88.9	86.1	79.8	74.2

Table 3: Primary load maximum stress values for SS 316L annealed alloy under Level A. Level D criteria: minimum value between [2.4∗ S_m] or [0.7∗ (R_m)min]

100 ^{o}C					
D (dpa)	2.75	3	3.5	5	10
S_{em}^A (MPa)	3711	3525	3153	2038	552
S_{et}^A (MPa)	6371	6072	5474	3680	1275
S_{em}^D (MPa)	6872	6528	5840	3775	1022
S_{et}^D (MPa)	11798	11244	10137	6816	2361
200 ^{o}C					
D (dpa)	2.75	3	3.5	5	10
S_{em}^A (MPa)	3257	3097	2777	1817	536
S_{et}^A (MPa)	5600	5344	4832	3295	1231
S_{em}^D (MPa)	6032	5735	5143	3364	993
S_{et}^D (MPa)	10371	9897	8948	6102	2279
300-350 ^{o}C					
D (dpa)	2.75	3	3.5	5	10
S_{em}^A (MPa)	2827	2674	2367	1447	294
S_{et}^A (MPa)	4849	4602	4108	2626	472
S_{em}^D (MPa)	5235	4951	4384	2680	544
S_{et}^D (MPa)	8980	8523	7608	4863	874
400-550 ^{o}C					
D (dpa)	2.75	3	3.5	5	10
S_{em}^A (MPa)	1957	1752	1340	140	140
S_{et}^A (MPa)	3424	3093	2432	316	316
S_{em}^D (MPa)	3625	3244	2481	259	259
S_{et}^D (MPa)	6341	5728	4503	586	586

Table 4: Secondary load maximum stress values for SS 316L annealed alloy under Level A and Level D criterias

5 Methodology

5.1 Particle transport analysis

The radiation transport analysis in complex geometries needs several codes, software and tools to be implemented. This study combines the software *SuperMCAM or MCAD* [15], the codes *MCNPX/6* [18] and *ACAB 2008* [17], and the tool developed by the ESS Bilbao Team *GIGANT* [16]:

- ◇ *SuperMCAM or MCAD:* software to convert CAD geometries to MCNP format and other codes.
- ◇ *MCNPX/6:* general-purpose Monte Carlo N-Particle code that can be used for particles transport.
- ◇ *ACAB 2008:* computer program designed to perform activation and transmutation calculations for nuclear applications.
- ◇ *GIGANT:* (General Implemented Geometry Activation Neutron Tool) developed to implement complex geometries for activation calculations.

The methodology used to reach the results is shown in Figure 4, which summarizes the followed process.

The first step is to transform the CAD geometry into the format used in the code for particles transport, MCNP. The software that does the transformation is SuperMCAM.

The initial geometry has to be modified and simplified in order to make it easily to transform and simulate with the Monte Carlo code. In a general way, the simplification consists on remove or change the elements that are dispensable, from the neutron transport point of view. Some of these elements are bolts, nuts or chamfers. Moreover, several types of geometries are not able to be transformed to MCNP format, like spirals or surfaces defined with sketches.

The target model transformed by SuperMCAM has been implemented in the ESS Target Station model for MCNP. This model includes a detailed geometry of the target and the shaft with the final helix shape, which are the most important components for the analysis.

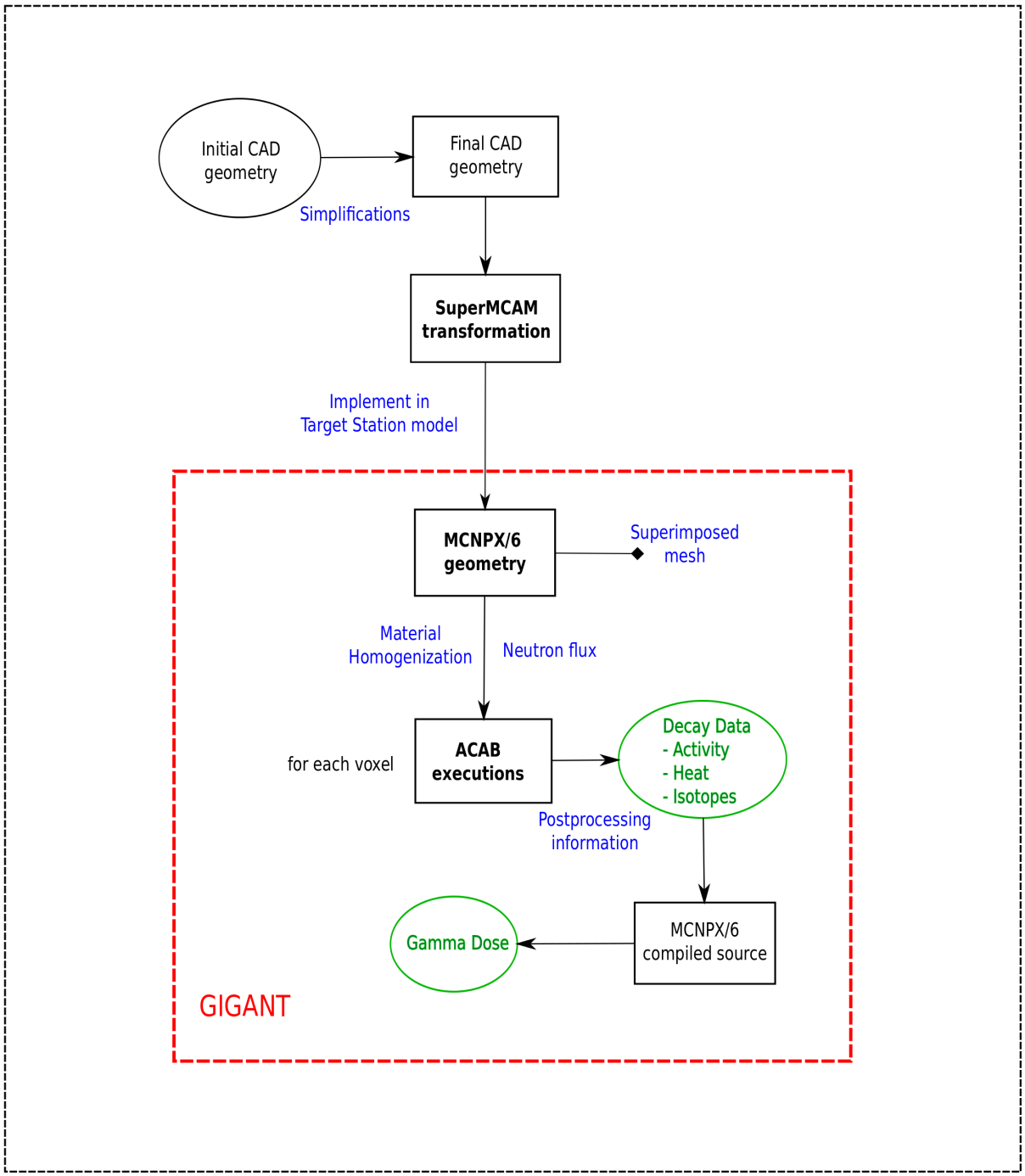

Figure 4: Scheme followed in the calculations from the initial CAD model to the final results.

Figure 5 shows the MCNPX model for the target spallation material. A detailed geometry for

one sector has been included, in order to produce high accuracy results for heat load, irradiation damage and streaming proton paths along the wheel. The remaining 35 sectors has been simplify as an homogeneous mixture of helium and tungsten keeping the average density. Details on the model can be found in ESS Document

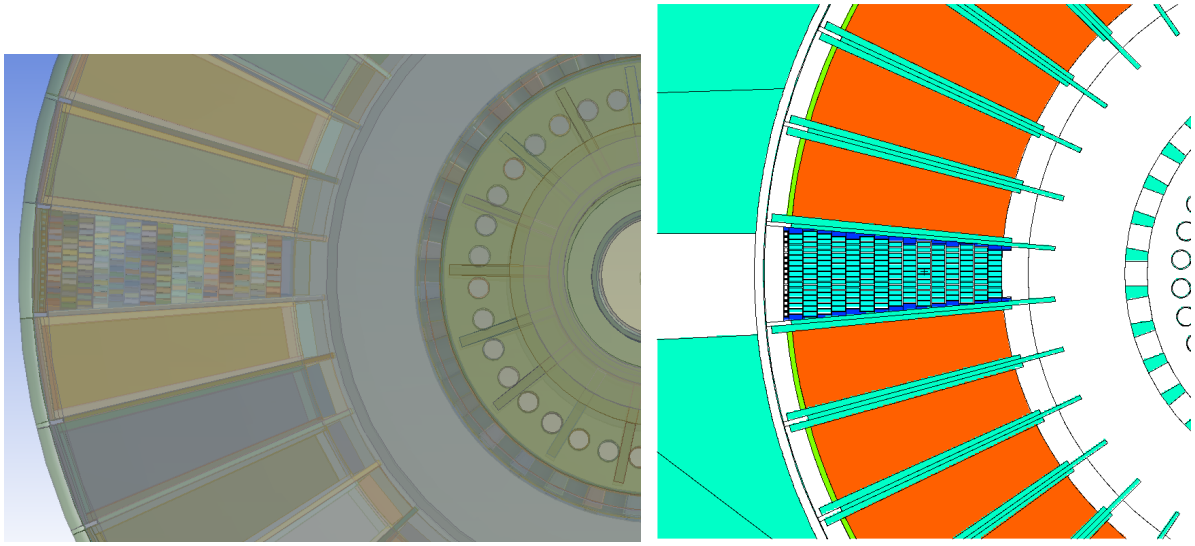

Figure 5: Geometry transformation from CAD model to MCNP format for ESS Target.

5.2 Particle transport model for SF2: Wheel-beam desynchronization

The model described on section 5.1 have to be rotate in order to reproduce the heat load conditions associated to the worse scenario for desynchronization. In this scenario the beam impacts on the rib after a 5^o rotation of the target geometry.

Regarding the spallation material is has been homogenised is order to reduce the computing time. The final model is shown on Figure 6.

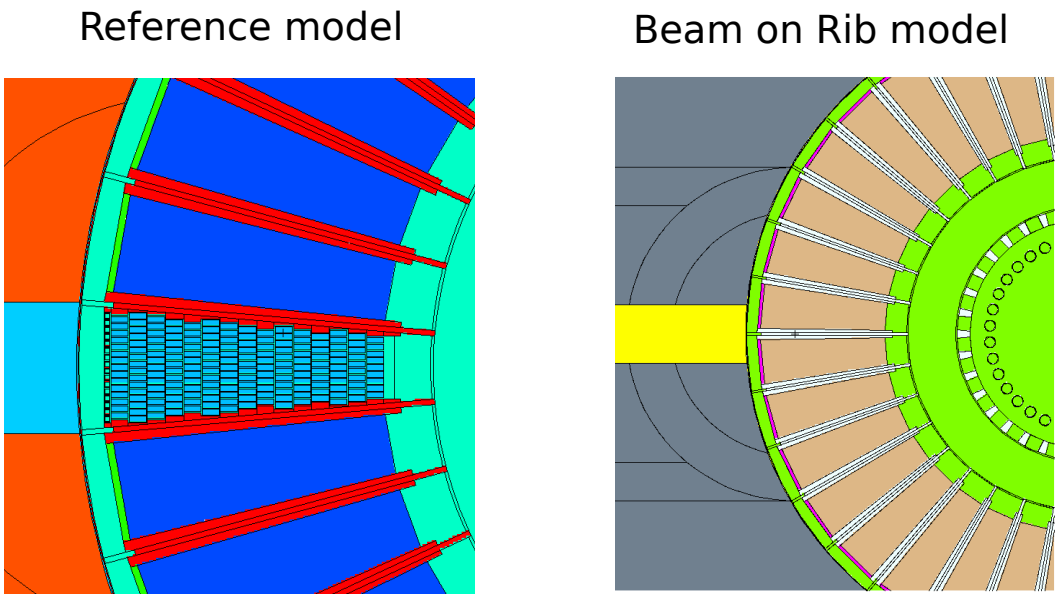

Figure 6: MCNP model for Wheel-beram desynchronization.

5.3 Residual heat spatial distribution

The residual heat analysis has been performed according to the procedure and models described on [33].

5.4 FEM-Mechanical model

The temperature distributions evaluated by means of the FEM-Thermal model (See section 5.5) are considered as thermal loads for the mechanical analysis (secondary load). This section describes the finite element mechanical model considered to evaluate the stress profiles in the Target Vessel.

The analysis is performed by means of an mechanical steady state model (linear analysis or elastoplastic). The geometry includes two "half" sectors in order to reproduce properly the stress distribution in the rib area. The following boundary conditions are considered:

- Fixed support in the flange between shaft and wheel (B)
- Dead weight (A)
- Internal pressure (C,D)
- Cassette and tungsten weight (E)
- Symmetry planes

Figure 7 summarized the primary loads taken into account for the mechanical analysis. Regarding secondary loads, only temperature distributions evaluated with FEM-Thermal model described on section 5.5 are considered.

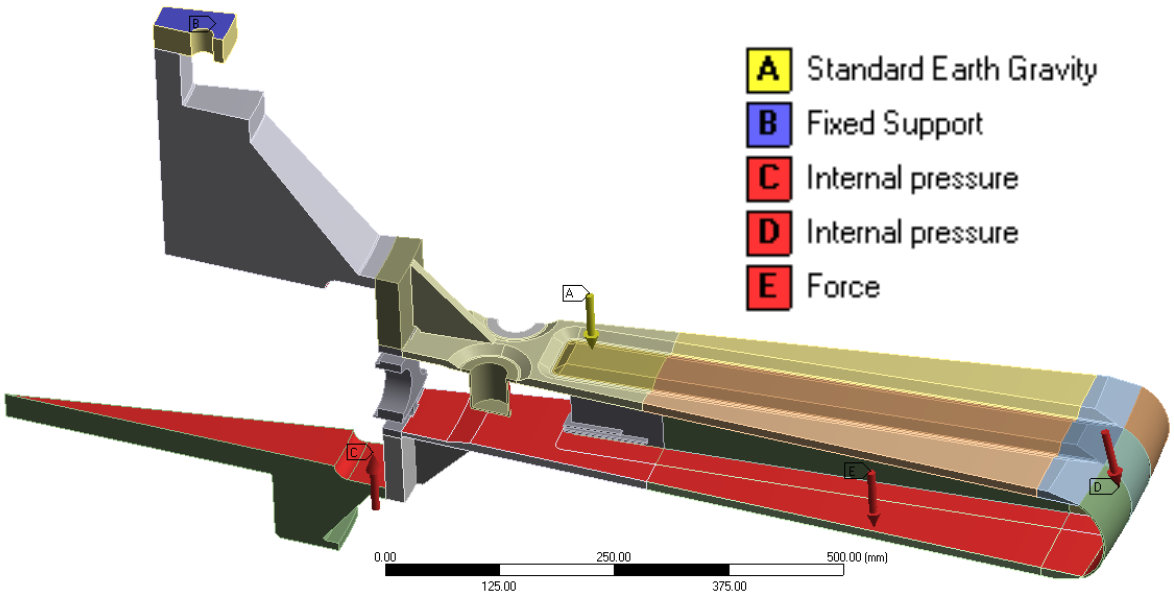

Figure 7: Primary loads in the internal structure

With regard to the mesh, a conformal mesh composed by 62.794 elements was employed. Figure 8 shows the mechanical mesh. The model includes at least two elements in the thickness of the shroud and only one element in the PBEW. In the PBEW, one element is consider enough because the stress profile is homogeneous and stress concentrators are not shown.

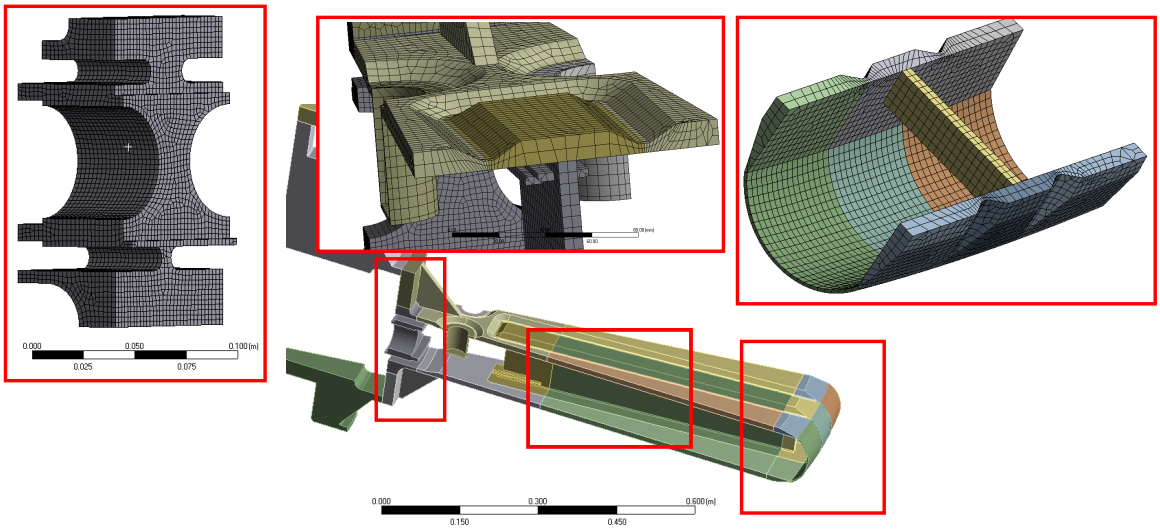

Figure 8: Mesh used to evaluate the mechanical stress profile on the Target Vessel

5.5 FEM-Thermal model

The FEM-Thermal model described in this section was employed to obtain the Target Vessel temperature profile evolution during the proton pulse heating and subsequent cooling once the steady state conditions has been reached.

The Cassette plates and Spalation Material were removed from the model and taken into account through boundary conditions in the interface surfaces. The FEM-thermal model is consistent with the FEM-Mechanical model described on previous section 5.4.

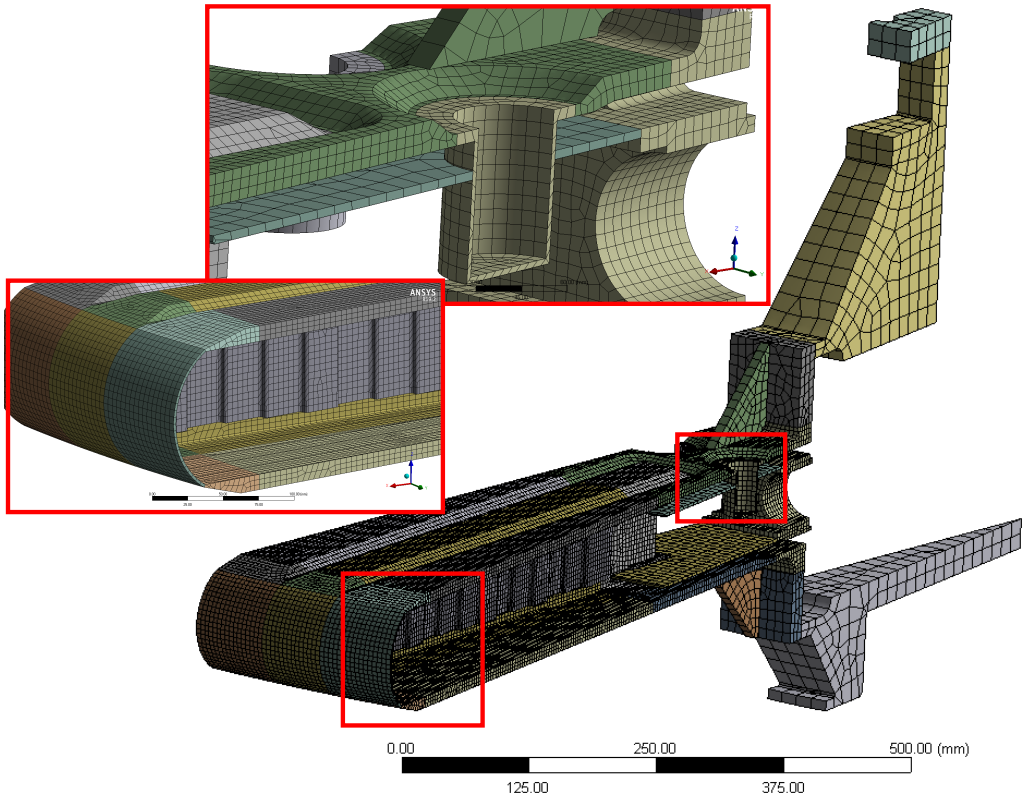

Figure 9: ESS Target Vessel geometry and mesh employed in the Thermal FEA for SF1 conditions.

The FEM-Thermal model mesh (Figure 9) consist on a non-conformal hybrid mesh which is constituted mainly by second-order hexahedral elements. Mesh metrics are detailed in the table 5.5.

Mesh metric	Average value
Elements	79737
Orthogonal quality	0.64
Skewness	0.45
Aspect ratio	5.6

Table 5: ESS Target Vessel FEM-Thermal model mesh metrics.

The methodology followed to obtain the Target Vessel temperature profile evolution during a pulse and subsequent cooling is shown in the Figure 10 and consist of the steps described below:

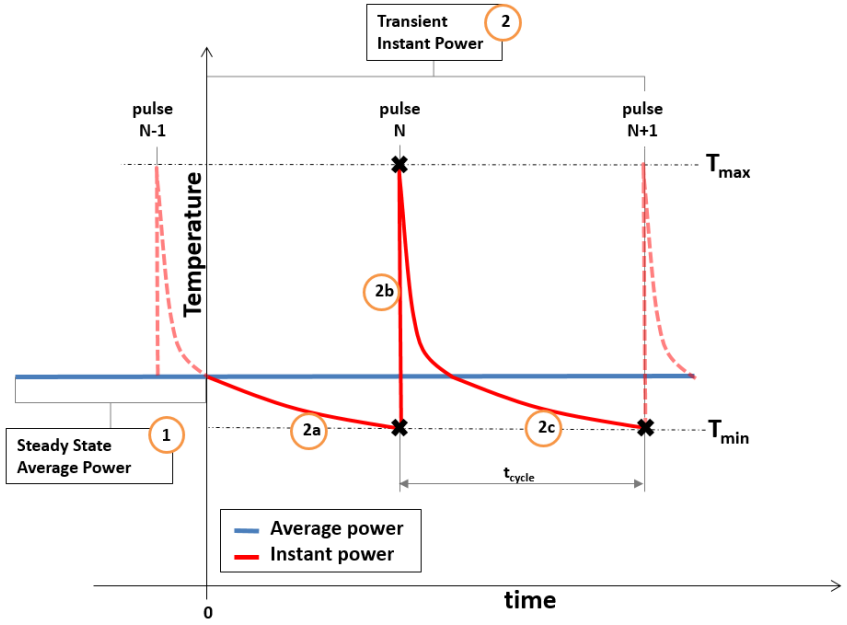

Figure 10: Target Vessel Thermal analysis methodology for SF1 conditions

- Step 1: Is an Steady state analysis is solved employing the time averaged heat load which is defined in ESS-0034495 [29], also the beam power is normalised to 5.2 MW.

- Step 2: Is a transient analysis which is divided in three sub-steps:
  - Steady state temperature at average power from step 1 is taken as initial condition, for this reason half of the period in between pulses ($t_{cool}/2$) the source is off (2a) in order to reproduce the cooling process between pulses.
  - After this period, the heat source is activated (2b) in order to reproduce the temperature increase during the pulse, the instant heat source has the same profile as the average but multiplied by the number of sectors and divided by the duty cycle.

The Target Vessel temperature profile at the end of this sub-step is employed for the fatigue analysis of the component.

– In the sub-step 2c the source is off during the cycle cooling time (t_{cool}). The Target Vessel temperature profile at the end of this sub-step is employed for the fatigue analysis of the component.

This process allow to reproduce the temperature distribution in the target at two extreme conditions: the end of the cooling period (minimum temperature) and at the end of the pulse (maximum temperature).

Regarding boundary conditions, the following are considered:

- Convection: Heat transfer coefficient (h) and helium temperature (T_He) were obtained from the Target Vessel and Shaft CFD model which is described in the document ESS-0066301 [8].The convection boundary condition is applied in the fluid-solid interface. As considered in the ESS Spallation Material and Cassettes FEM thermal [23] the cooling BC can be considered no time-dependant once reached the nominal operation conditions in the Target, which makes this BC suitable for both steady state and transient analysis.

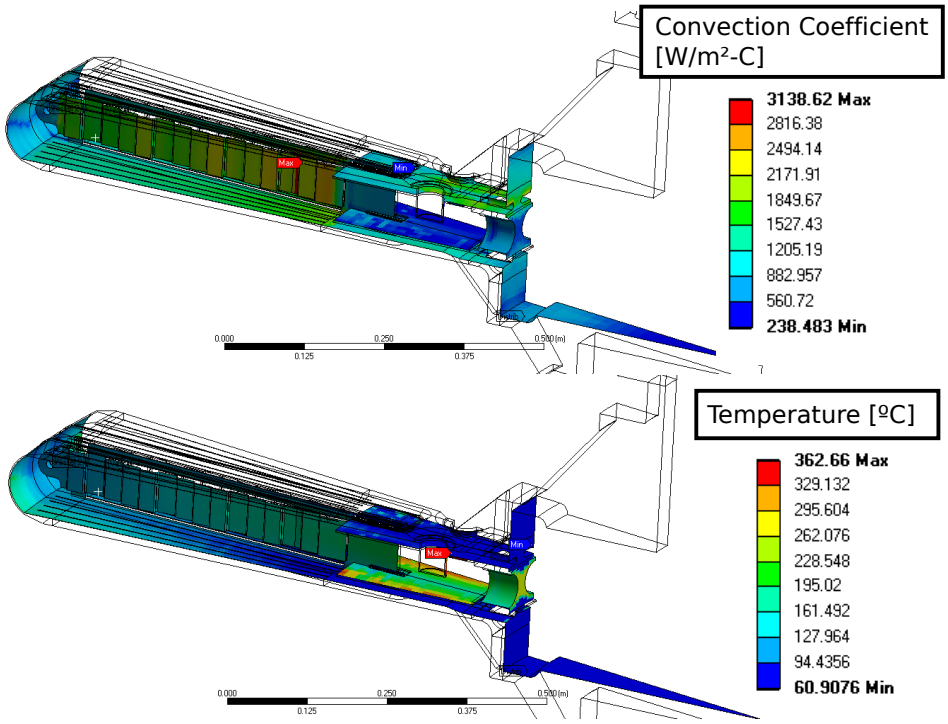

Figure 11: Target Vessel FEM-Thermal model cooling convection boundary conditions for SF1 nominal load scenario.

- Thermal contacts: Perfect thermal contact was considered between different parts of the model that are welded, however a 25000 W/m^{2}K thermal contact conductance was set

on the vessel rib-cassette side contact interface to reproduce the helium between both components.

- Adiabatic: The external surface of the Target Vessel was considered an adiabatic surface which is a conservative assumption.
- Symmetry: Due to the ESS Vessel geometry and loads conditions for the SF1 load scenario 1/36 symmetry can be assumed which corresponds to two half sectors as shown in Figure 9. This assumption will considerably reduce the computational time and resources without compromising accuracy.

5.6 FEM-thermal model for shut-down analysis

The shutdown scenario describe on section 8.5 considers a case in which the beam is off shutdown and the coolant flow is interrupted. In this conditions the residual heat have to be evacuated by means of conduction between bodies and thermal radiation. Obviously, the helium inside the target establishes convection between tungsten bricks, however, the small size of the gaps in between bricks will reduce its effect. Based on that, we propose a conservative scenario in with there is only heat transmission between solid bodies.

The FEM consider is based on the FEM-Thermal model shown on Section 5.5 in which we have include two stainless steel plates connected in from of the vessel to simulate the shielding conditions. The bottom plate is bounded to the cassette taking into account that gravity will guaranty a good thermal contact. In the cassette of the connection which the top plate a thermal resistance equivalent to 1 mm helium gab is included.

Regarding the heat generation profile, only spallation material is considered as decay heat source. A detail description of the evaluation process is shown on Section 7. Finally, the vessel removes the heat by radiation on its external surfaces (shielding).

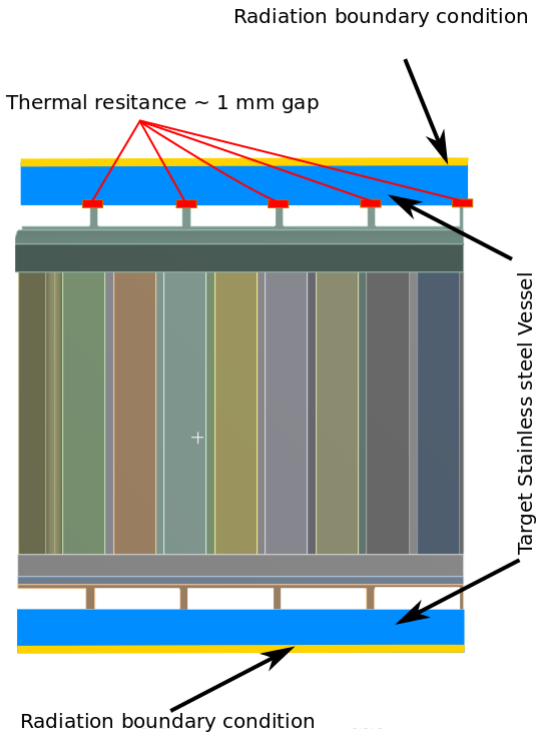

Figure 12: Thermal resistances and boundary conditions for the shutdown case

Three accidental cases related to beam malfunctions have been studied. Considering only the

beam shape and generation, two main problems can appear:

- Losing the raster.
- Focusing the beam.

These lead to the three following scenarios that will be studied:

1. Rastered and focused beam
2. Unrastered but nominal beam
3. Unrastered and focused beam

5.7 Wheel-Beam desynchronization

This section describes the methodology employed to evaluate the thermomechanical behavior of the ESS Target Wheel on worst case wheel-beam desynchronization scenario. The Target Wheel has reached the steady state working under the design conditions (SF1 load scenario) when desynchronization occurs and the pulse beam begins hitting on the Target rib center as shown in Figure 13.

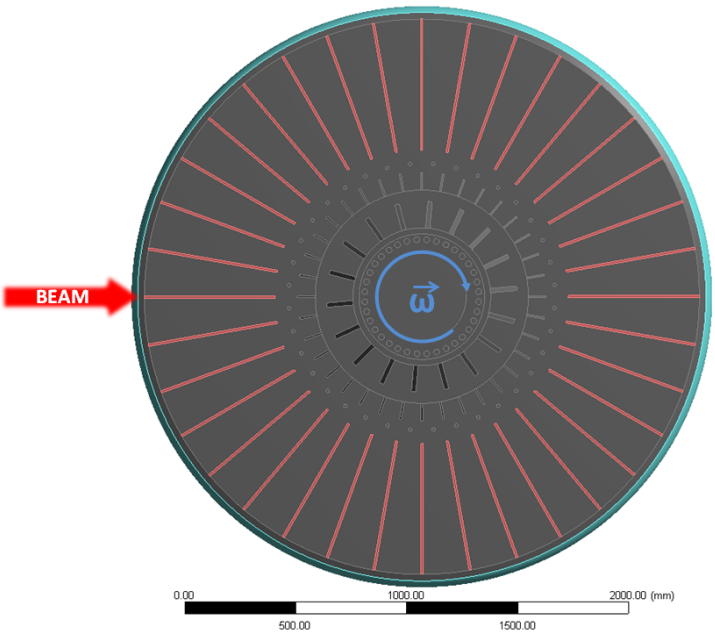

Figure 13: Wheel-Beam desynchronization load scenario

For the evaluation of this load case scenario different CFD simulations were solved using the Target Wheel sub-model 2 described on the document ESS-0066301 [8]: Target, Shaft and

Rotating seal CFD analysis.The manufacturing path including calibrated plates ajustement [34] hence, good contact beetween cassette and rib is considered (U=25000 W/m^2K).

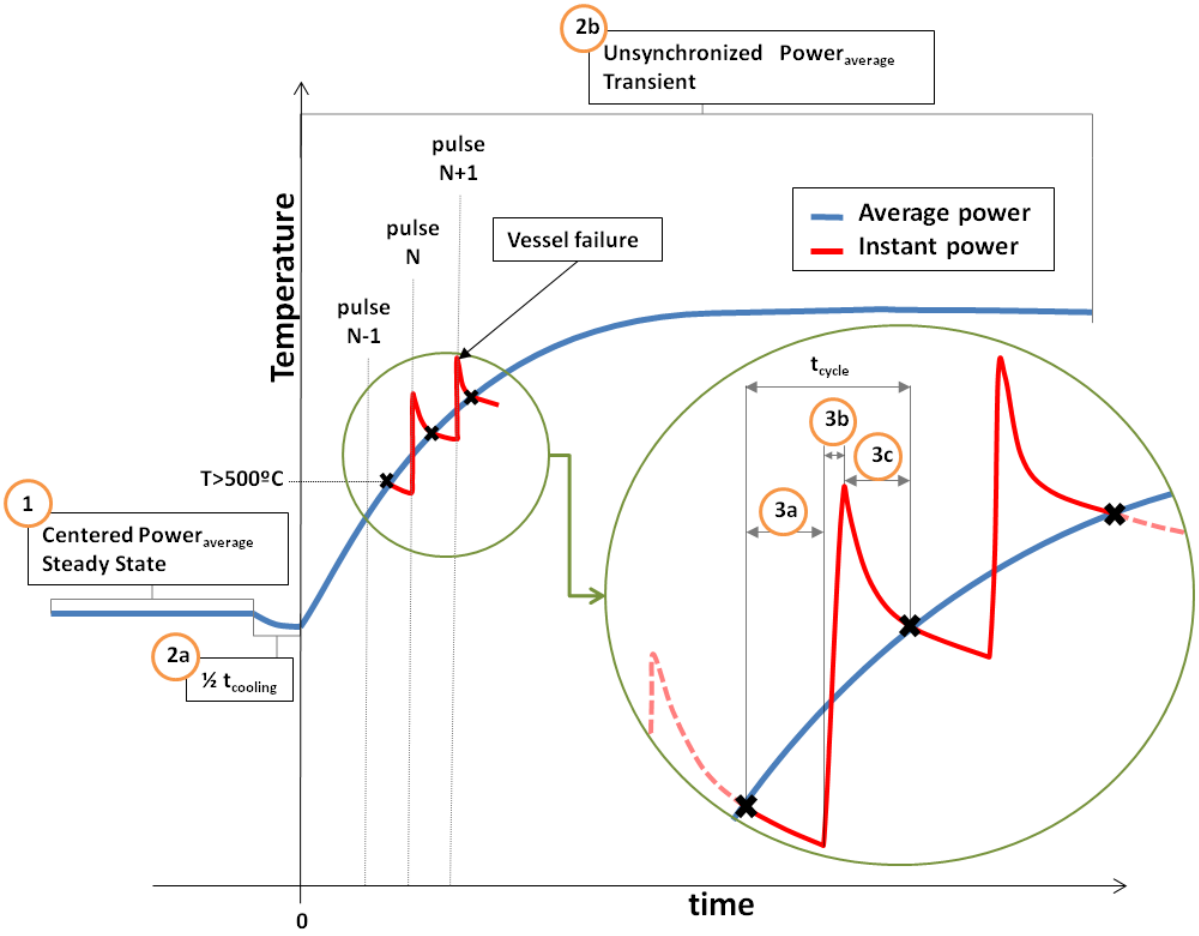

Figure 14: Methodology scheme for solving the SF2 Wheel-Beam desynchronization load scenario

The employed methodology is described in Figure 14 and consist on the following steps for each thermal contact condition:

1. In order to get the initial conditions a steady state CFD simulation at the average beam power is solved. Just before the Wheel-Beam desynchronization, the ESS Target has reached the steady state working under the SF1 load scenario described on section8.2.

2. A CFD transient in the new beam conditions at average beam power is performed. This analysis shows the time average evolution of the temperatures during the next 50 s until the temperature of the shroud achieves 500^oC. The thermal transients in the stainless steel will produce temperature fluctuations in the range of 30^oC and thus they are not relevant.

3. The temperature distribution achieved when maximum temperature exceeds the 500^oC will be the imput the secondary loads analysis.

6 Radiation damage conditions

The nuclear reactions produced on the spallation material will generate a large amount of neutrons. These neutrons has enough energy to produce displacements in the metallic meshes of the elements close to the source. The accumulation of this displacements degrades the mechanical properties of the material.

The Target vessel is one of the closest elements to the spallation material hence, the damage produced by neutrons play a role in its mechanical behavior. The methodology proposed for the evaluation of the radiation damage is described in not in the scope of this document, however several conclusions based on previous analysis are remarkable[19]:

- High energy neutrons will produce nuclear cascades similar to neutrons considered on $RCC - MR_x$ damage analysis methodology
- Ratio Helio/DPA in the elements not in contact with the proton beam are comparable with fission reactors
- Helium and hydrogen production are far below values that can produce mechanical effects.
- The faction of disperse protons that produces damage in the cassette is negligible compared with neutron damage.

Based on this assumptions, the model described on section 5.2 has been evaluated with KIT damage cross sections for steel [22].

It should be remarked that the model reproduces the damage profile considering a perfect synchronization between accelerator and target for the 5 years of operation. This operation mode maximizes the damage in the center of the top and bottom plates and minimizes the damage in the ribs as it can be shown on Figures 15. The damage level in the Top and bottom covers of the vessel will be 3 dpa and the level in the rib is close to 1.2 dpa.

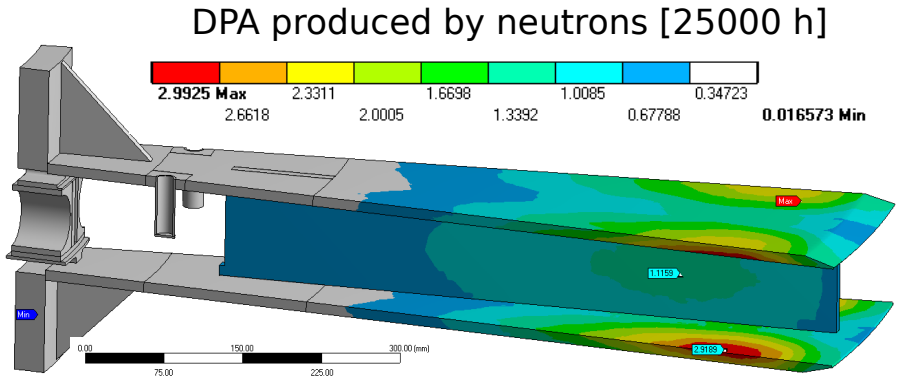

Figure 15: DPA produced on the Target Vessel for 25 kh of operation at nominal beam conditions [dpa]

Regarding BEW, the maximum damage will be 3.5 dpa considering protons and neutrons as it is shown on Figure 16. This region has to be consider according to $RCC-MR_x$ as an irradiated area.

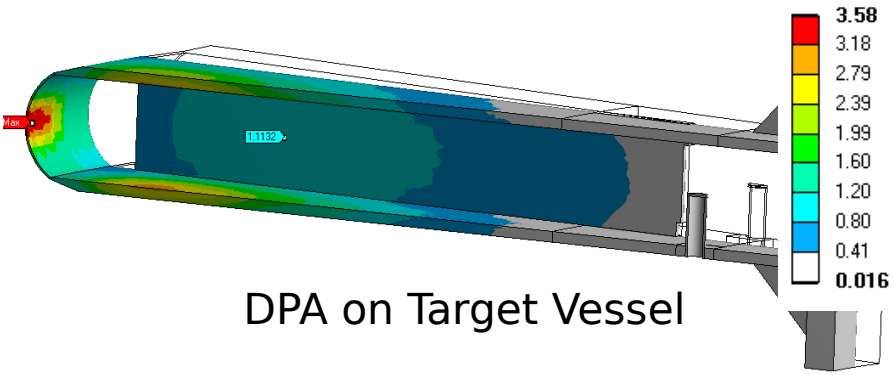

Figure 16: DPA produced on the Target Vessel for 25 kh of operation at nominal beam conditions [dpa]

7 Residual heat and inventory

The residual heat analysis is summarized on report [33].

8 Load scenarios thermomechanical analysis

8.1 SF1: Design conditions

The Design conditions are considered a load scenario in with maximum overpressure in the helium loop (13 bar(g)) is produced at the same time as the maximum temperature in the Target Vessel (500^o C) as it is described on Section 2. Despite of the fact that this conditions are not going to be produced on normal operational conditions, a protection level A has been define for this scenario base on licensing aspects [1].

The following sections shows the mechanical analysis according to $RCC - MR_X$ rules taking into account that no secondary loads or S-damages will be produced.

P damage analysis

The Design loads produce unclear results for elastic analysis hence and elastoplastic evaluation is proposed. In order to carried out this analysis, a elastoplastic model is consider to reproduce the material behavior at 500^oC. Mechanical properties for plastic model has been evaluated according to "minimum curves" described on apendix A3.3S.45 from $RCC - MR_x$ 2012.

According to section RB 3251.114, the analysis have to be performed multiplying all the loads of the system by 1.5 coefficient (Protection level A) and excessive deformation should not be produced. Following the criteria proposed on section RB 3121.1, excessive deformation is produced when the overall permanent deformation exceeds the deformation which would occur with purely elastic behavior. Figures 17, 18 and 19 shows the maximum deformation in the pure elastic analysis, elastoplastic analysis and the offset deformation for the elastoplastic model. The offset deformation is lower than the pure elastic deformation thus, the design fulfill the elastoplastic criteria.

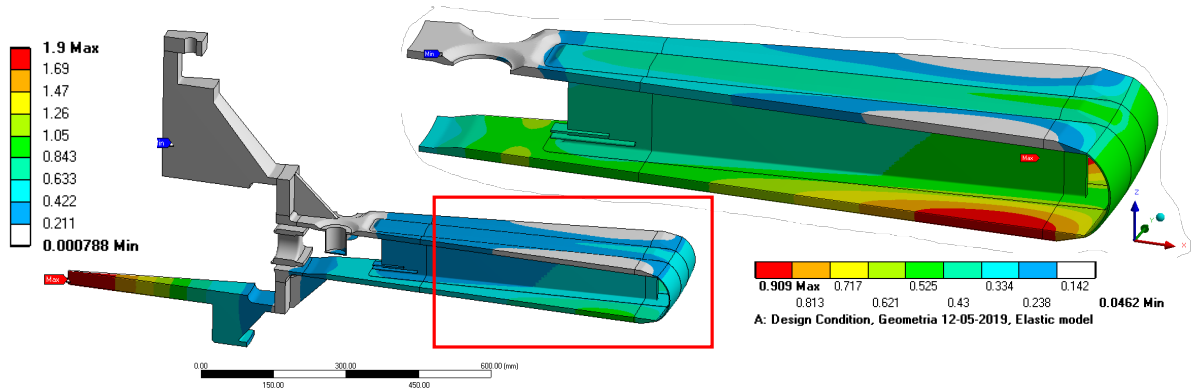

Figure 17: Deformation for pure elastic analysis for 1.5 design loads.

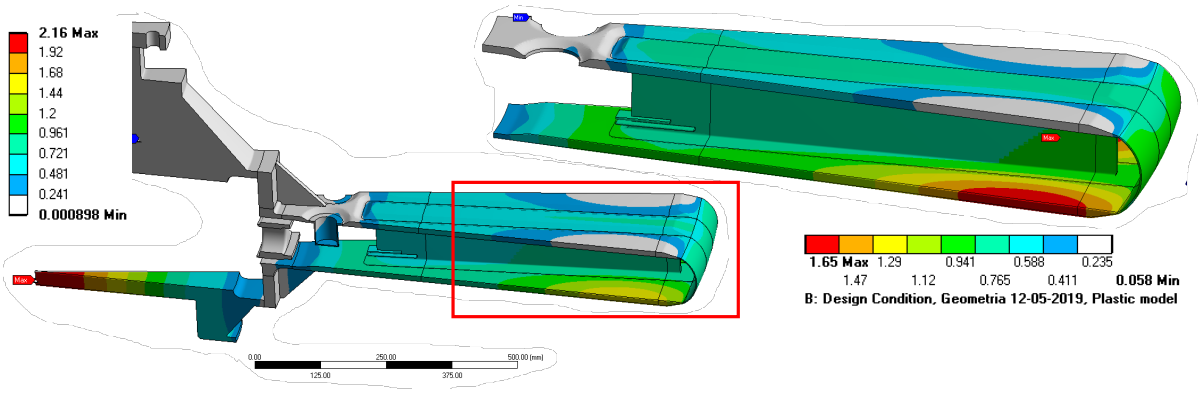

Figure 18: Deformation for elastoplastic analysis for 19.5 bar(g) (Loads multiplied by 1.5)

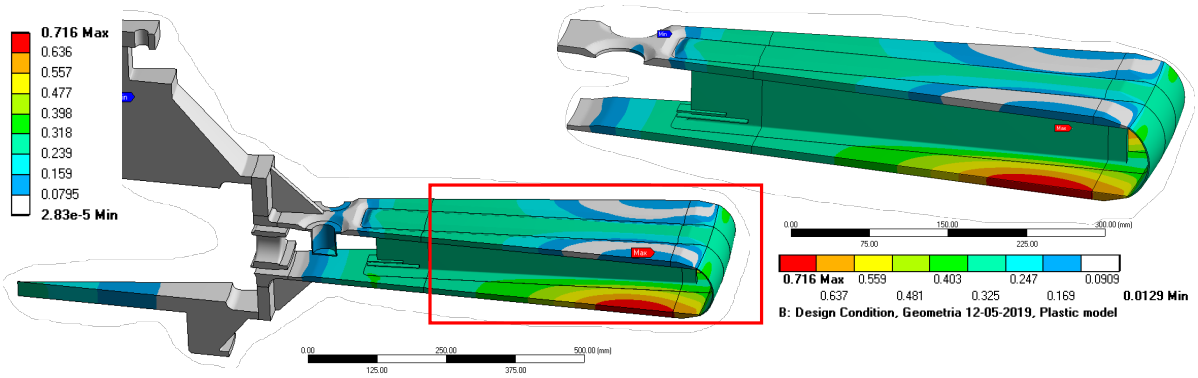

Figure 19: Offset deformation for elastoplastic analysis for 1.5 design loads.

S damage analysis

Design conditions do not produce any cyclic load hence, S damage analysis is not needed.

8.2 SF1: Nominal conditions

Based on the description showed on Section 2, nominal conditions (A01) are produced by the design beam (nominal shape, energy and repetition rate) hitting the wheel at his nominal rotation speed. Also the beam is considered synchronized with the wheel and hitting in the center of the section. The cooling system is working at nominal conditions, so helium mass flow trough the wheel is 2.85 kg/s. Figure 20 shows the beam on nominal conditions. The Design beam for nominal conditions includes the uncertainty on beam instrumentation, which means 20% more concentrated beam than expected one. Table 6 shows the main beam parameters for this load case.

Parameter	**Units**	**Value**
Beam Energy	GeV	2.0
Maximum Beam Energy	GeV	2.2
Pulse Repetition Rate	Hz	14
Beam energy per pulse	kJ	357
Maximum Energy per pulse	kJ	371

Table 6: Main beam parameters[5]

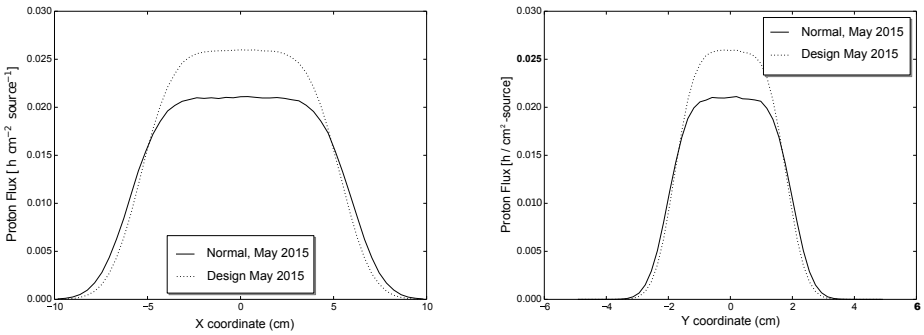

Figure 20: Nominal Beam and design beam[5].

Following the $RCC - MR_x$ mechanical design rules, the loads have been classified as Primary (Pressure and dead weights) and Secondary (thermal stresses) and on critical sections linearized analysis has been perform. Next sections will describe the analysis of the component to prevent P and S damages.

8.2.1 Heat load

The heat load for this load scenario was obtained using the target station MCNP model described on section 5.1 and is based on the design beam footprint, defined in ESS-0003310 [5] and ESS-0034495 [29] also it is normalised to 5.2 MW. Table 7 includes the maximum power density generated by the proton beam and the total power at each zone of the model for SF1 nominal conditions. The heat source values in the table are time averaged, the instant heat source is the same but multiplied by the number of sectors and divided by the duty cycle.

The volumetric heat load is transferred from MCNP external data files employing a triangulation weighted interpolation, the values at the FEM Thermal models are compared in Table 7. In figure 23 heat source zones can be identified, a external data file from MCMP was exported to each of these zones.

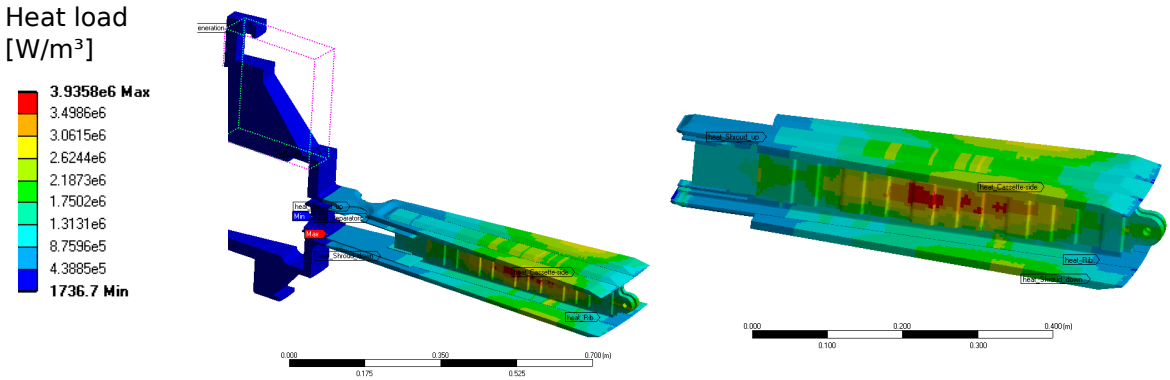

Figure 21: Time averaged power density load profile applied in the Target Vessel for SF1 nominal conditions considering that heat load is distributed in 36 sectors.

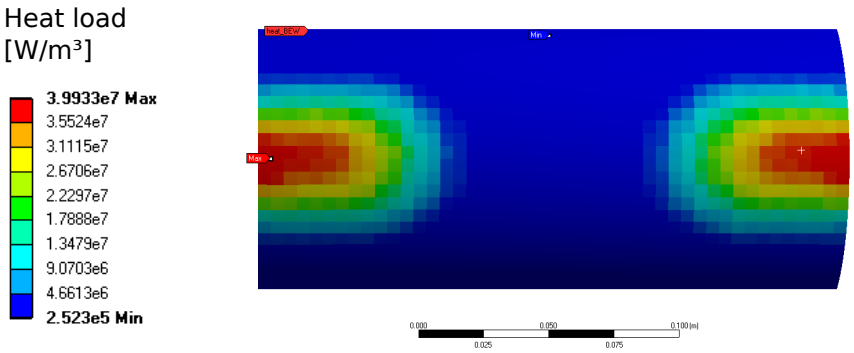

Figure 22: Time averaged power density load profile detail at Target Vessel PBEW for SF1 nominal conditions considering that heat load is distributed in 36 sectors.

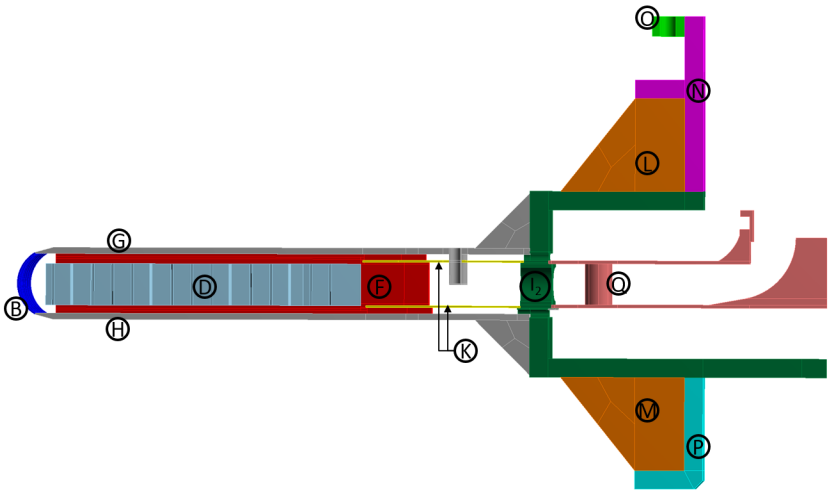

Figure 23: Target Vessel heat source zone division.

	Max Power Density (W/cm3) t-aver			Power deposition (kW) t-aver		
Zones	**MCNP**	**CFD**	**FEM**	**MCNP**	**CFD**	**FEM**
Tungsten	128,4	126,0	NA	2704,0	2678,3	NA
PBEW	36,8	39,5	36,5	12,9	12,7	12,9
Cassette_down	3,2	4,0	NA	24,1	24,1	NA
Cassette_side	2,5	3,4	3,9	48,3	48,6	48,3
Cassette_up	3,0	4,0	NA	25,1	25,2	NA
Shroud_up	3,6	2,8	2,8	68,5	67,7	68,5
Shroud_down	2,5	2,4	2,3	58,1	58,3	58,1
Rib	3,4	2,9	2,8	34,0	33,8	34,0
Cylinder_CFD	0,9	0,9	NA	-	5,5	NA
Cylinder_FEM	NA	NA	1,3	NA	NA	34,2
Separators	0,9	0,9	0,9	-	4,7	4,7
Dummies	42,1	38,4	NA	-	17,4	NA
Stiffeners_up	0,6	NA	0,7	3,6	NA	3,6
Stiffeners_down	0,6	NA	0,8	1,2	NA	1,2
Pipes_support_up	0,5	NA	0,6	5,9	NA	5,9
Pipes_support_down	0,6	NA	0,9	1,9	NA	1,9
Distributor	4,5	NA	4,5	-	NA	8,7
			TOTAL CFD MODEL	**2975,0**	**2976,2**	**-**
			TOTAL FEM MODEL	**271,0**	**-**	**282,0**

Table 7: Maximum power density and Power deposition by the design beam operating at SF1 conditions. TOTAL FEM model includes only the heat load in the shroud.

8.2.2 Temperature distribution

The ESS Target Vessel temperature evolution during a pulse and subsequent cooling was obtained employing the FEM-Thermal model and methodology described in section 5.5. Figure 24 shows the time average temperature profile once reached the steady state for SF1 nominal operation conditions.

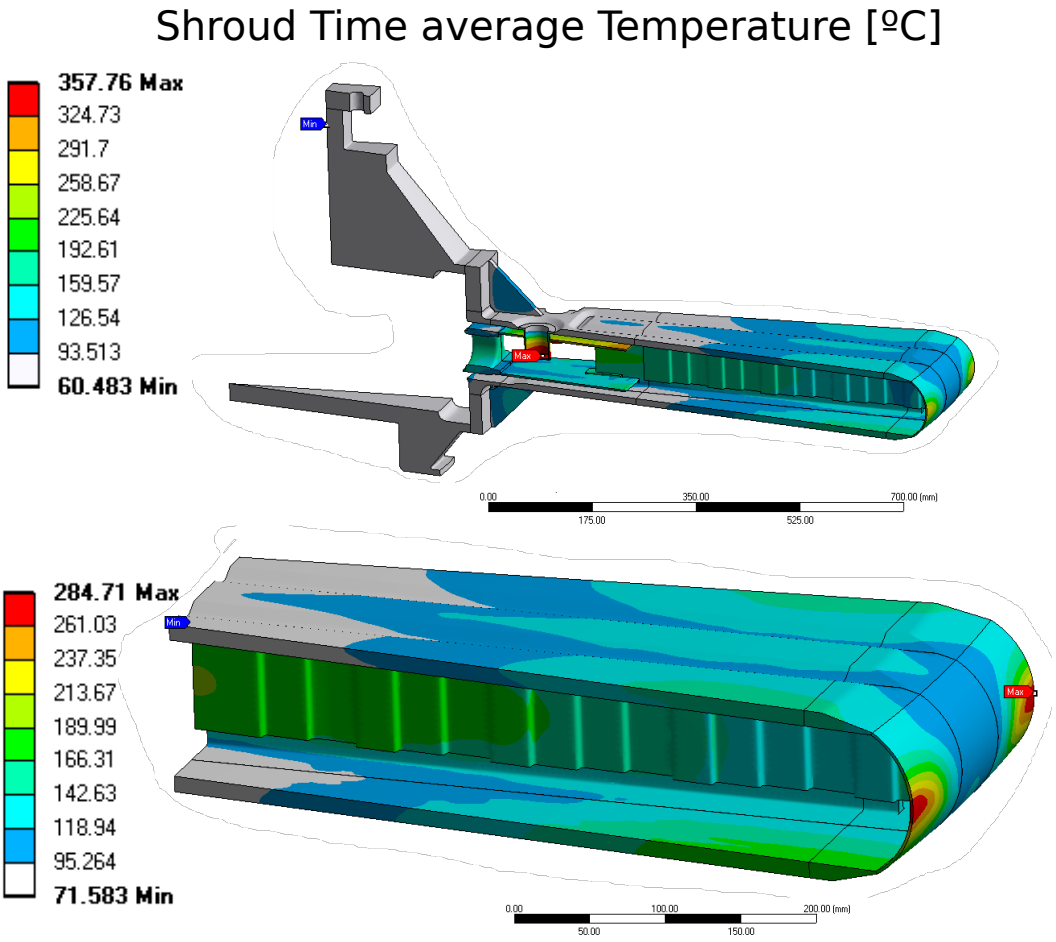

Figure 24: ESS Target Vessel temperature profile after the proton beam pulse for SF1 nominal conditions.

The Vessel shroud maximum temperature is reached in the probe cylinders in which the outlet helium impacts. The temperature at these locations remains around 360^{o}C. The temperature in the vessel do not change significantly during the pulse except in the PBEW (Figure 25) where the maximum heat deposition during the pulse is located. In this region the temperature increases 20^{o}C during the pulse. Figure 26 shows temperature evolution of the PBEW during

the pulse

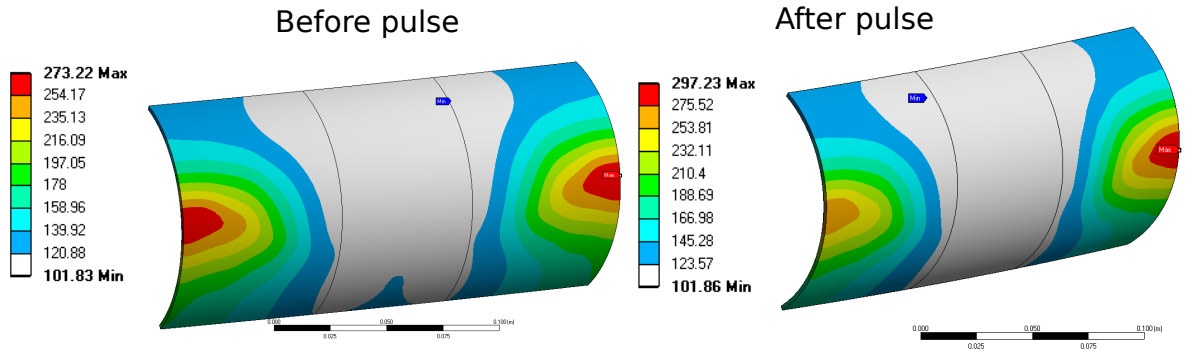

Figure 25: ESS Target Vessel Beam Entrance Window (PBEW) temperature profile before and after the proton beam pulse for SF1 nominal conditions

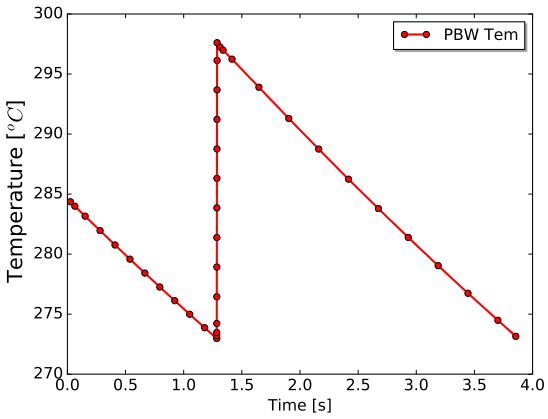

Figure 26: Target Vessel PBEW maximum temperature evolution once reached the steady operation for SF1 nominal conditions

8.2.3 P damage analysis

The analysis for P damage is based on the FEM mechanical model described on section 5.4 considering elastic properties for materials. Primary loads are produced by dead weights and the differential pressure between target vessel and monolith vacuum (12 bar(g)). Regarding secondary loads, the temperature distribution shown on previous section (after the pulse) is considered.

Primary loads

Figure 27 shows the Equivalent Von-Misses stress for primary loads (Dead weight and internal pressure). As it was expected, most of the geometry shows stress values below S_m however, there are areas in which stress concentration is shown and further analysis is needed.

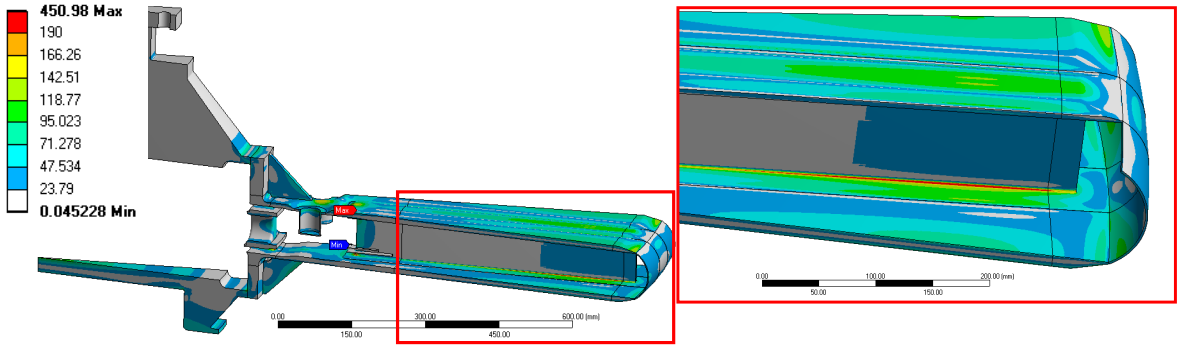

Figure 27: Equivalent Von Mises stress for primary loads

The higher stress values are shown in the back of Rib (Figure 28). Linealiced analysis is carried out to clarify the stress composition. The stress distribution along the shroud thickness (P1 on Figure 29) shows values in the range of 55 MPa P_m and 150 for $P_m + P_b$. In both cases the values are almost a factor of 1.8-2 lower that the acceptable limits at operational temperature ($P_m < S_m \sim 127MPa$ and $P_m + Pb < 1.5 \cdot S_m \sim 190.5$). Regarding the stress along the rib thickness (P2 on Figure 29) the membrane stress can be consider local according to RB 3251.112 (the area exceding 1.1 S_m is in the range of 4 mm < rib thickness). The $P_L \sim$ value is 127 MPa lower than the acceptable value ($P_L < 1.5 \cdot S_m \sim 184.5$).

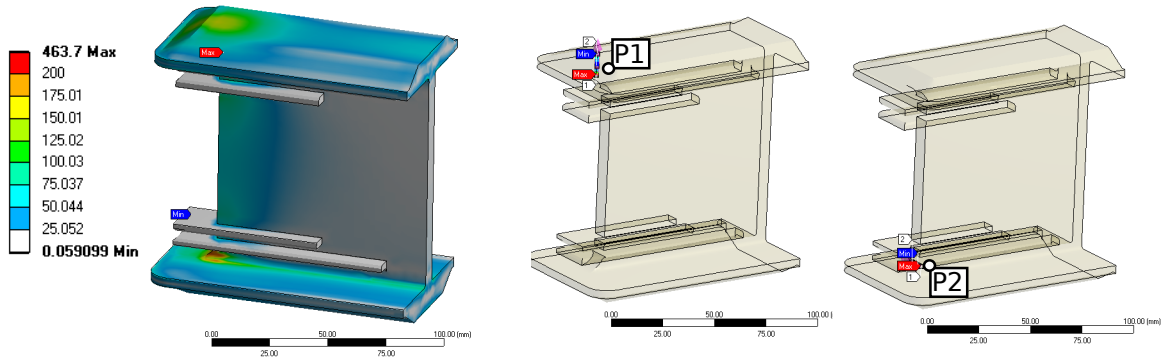

Figure 28: Equivalent Von Mises stress for primary loads in the back of the Rib

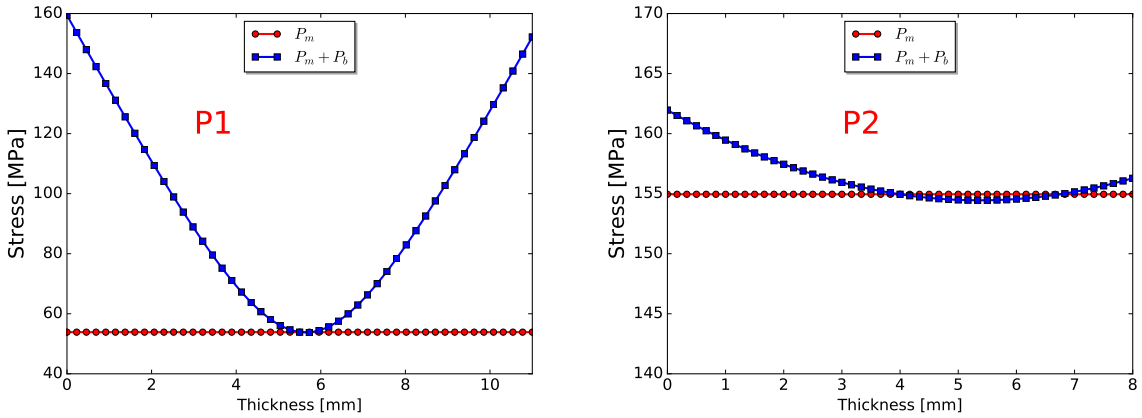

Figure 29: Equivalent Von Mises stress for linearized paths in the shroud thickness (P1) and in the Rib thickness (P2) (Figure 28)

The connection between the end of the rib and the beam entrance window shows high stresses. Figure 30 shows the stress distribution in the region. The end of the rib (P3 and P4) concentrates the stress produced by the vertical resultant forces in the PBW hence, linearized analysis is needed. The analysis of the stress composition (Figure 33) shows values in the range of 70 MPa P_m and below 180 for P_m+P_b ($P_m < S_m \sim 127MPa$ and $P_m+Pb < 1.5 \cdot S_m \sim 190.5$).

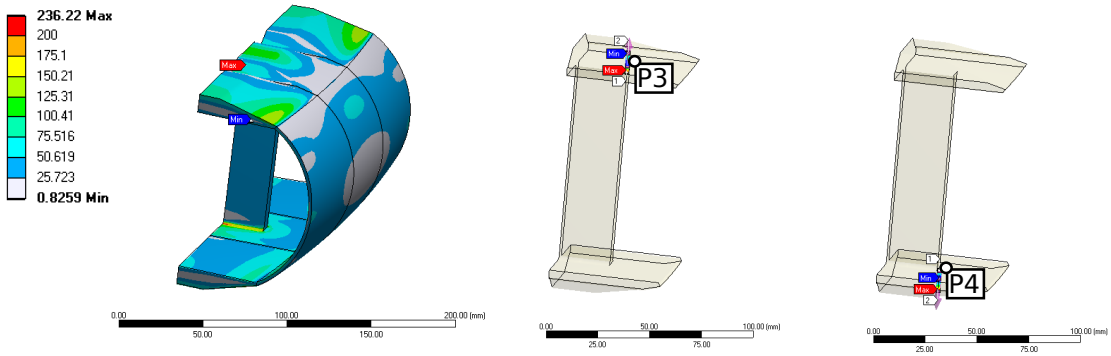

Figure 30: Equivalent Von Mises stress for primary loads in the back of the Rib

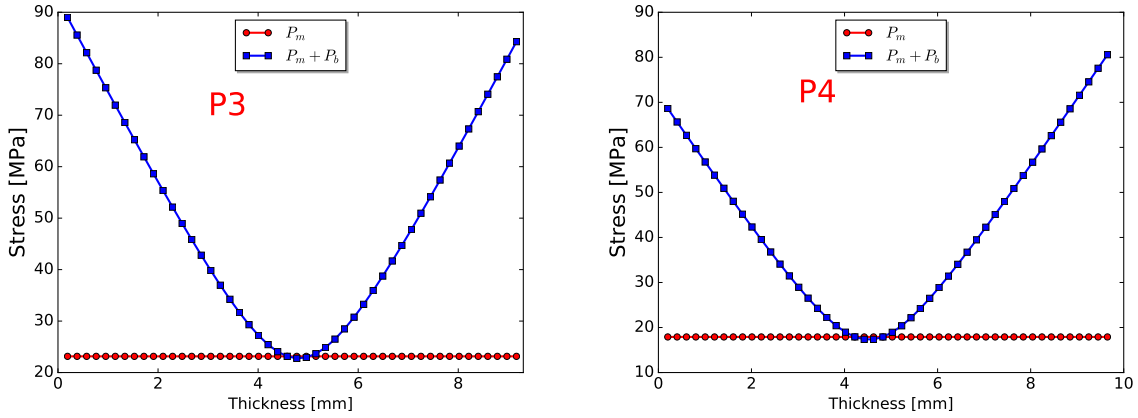

Figure 31: Equivalent Von Mises stress for linearized paths in the shroud thickness (P1) and in the Rib thickness (P2) (Figure 28)

Along the rib there is a clear line of stress produced by the bending of the shroud plates (Figure 32). The linearized path P5 is placed in the position closer to the corner of the rib. The analysis of the stress composition (Figure 33) shows values in the range of 25 MPa P_m and below 120 for $P_m + P_b$ ($P_m < S_m \sim 127MPa$ and $P_m + Pb < 1.5 \cdot S_m \sim 190.5$).

The path P6 is placed in the welding position. The distance between the welding line and the rib was selected to minimize the bending stress in the welding thus, the stress distribution shows almost no bending stress. The membrane stress (P_m) is higher that in other sections of the shroud due to the thickness reduction for the welding but still far from the limits of the

material ($P_m \sim 55$ MPa $< S_m$ 127 MPa). The stress values shown on the welding position are compatible with 0.5 welding coefficient which means that inspections are not needed to ensure the welding resistance. Nevertheless, surface inspection (visual and penetrant testing) and volumetric inspections (radio test) will be considered in the inspection plan.

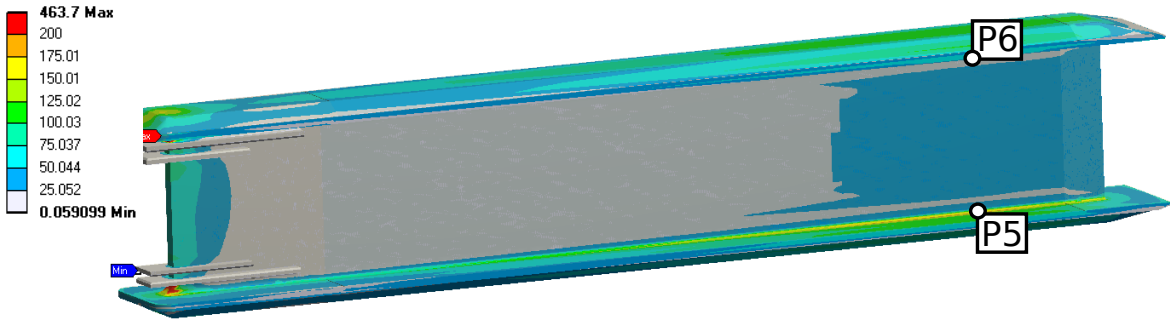

Figure 32: Equivalent Von Mises stress for primary loads in the center of the Rib

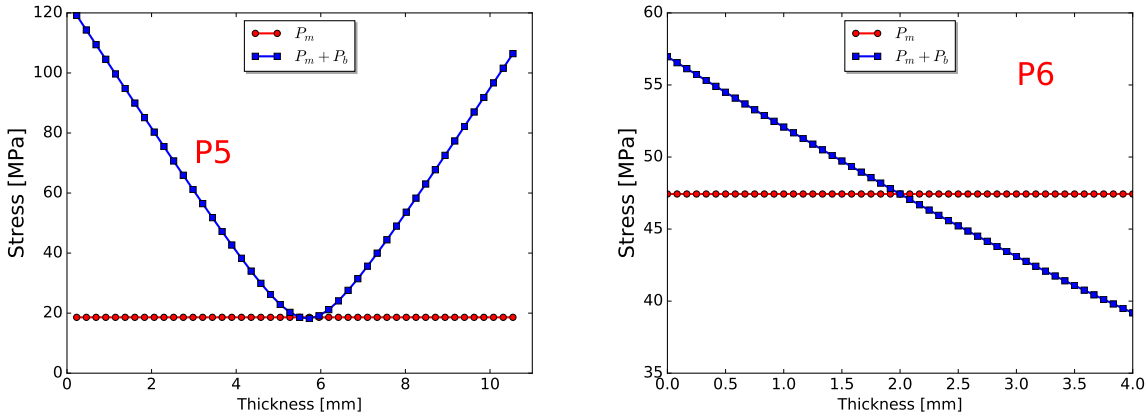

Figure 33: Equivalent Von Mises stress for linearized paths in the shroud thickness (P5) and in the welding thickness (P6) (Figure 32)

The connection between the shroud and the central axis is evaluated. Figure 34 shows the equivalent stress in the central axis. There are stress concentrations in the connection of the flange cover (P7) and the pedestal plate. It should be remark that a thickness reduction has

been introduced in both plates to reduce the welding thickness in the connection up to 15 mm. Both membrane stress and bending stress are far below the limits.

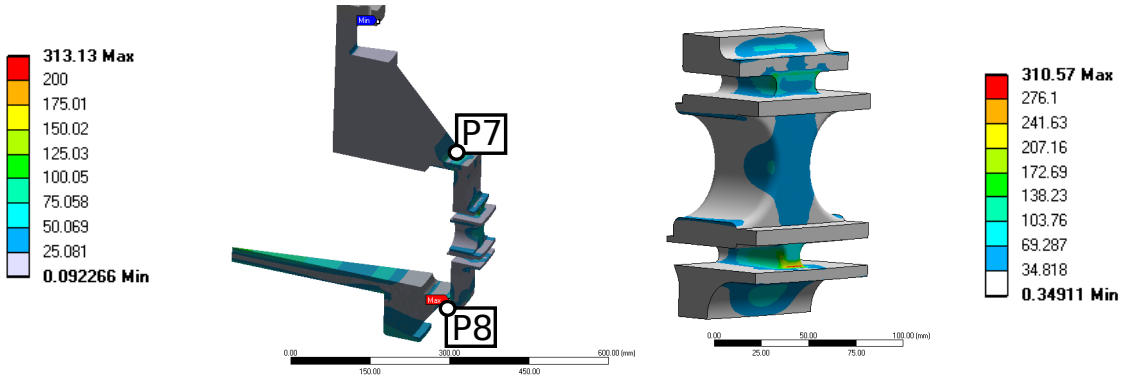

Figure 34: Equivalent Von Mises stress for primary loads in the central axis

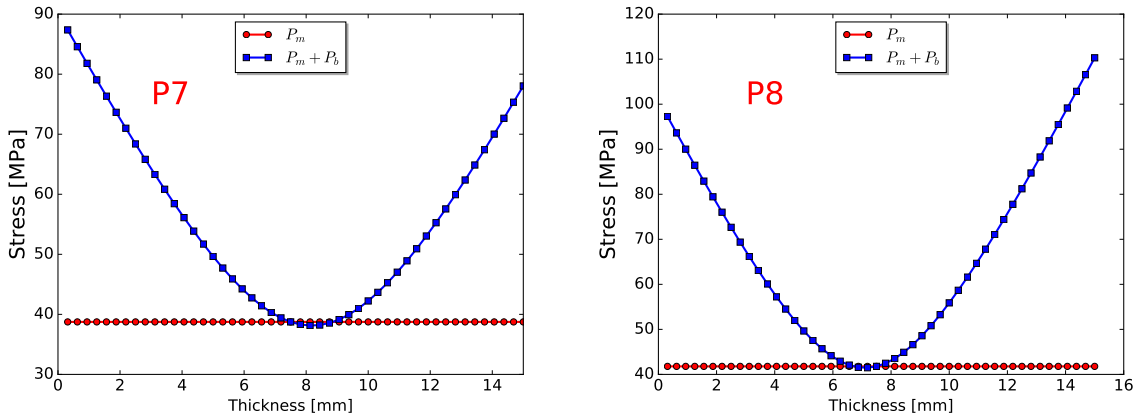

Figure 35: Equivalent Von Mises stress for primary loads in the central axis.

Finally, the axis inlet and outlet openings shows remarkable section reductions that increases the stress level. Figure 36 shows the equivalent stresses. According to the linearized analysis of the critical positions in the area (Figure 37) the stress levels are clearly below the stress limits.

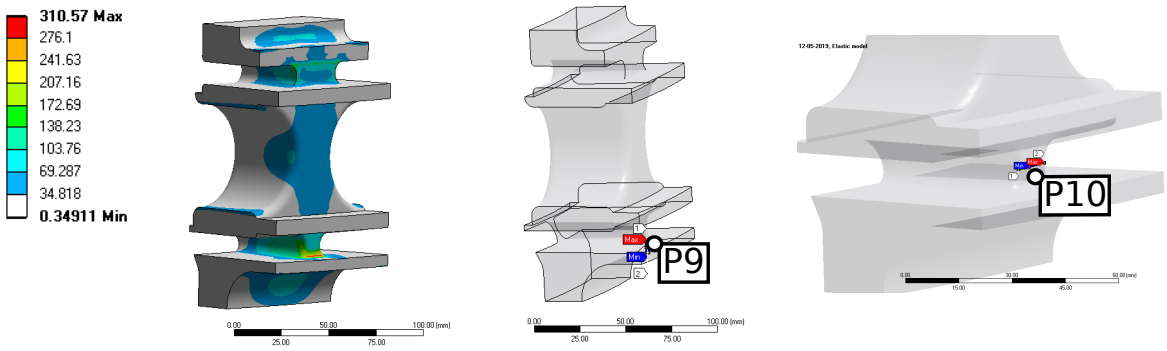

Figure 36: Equivalent Von Mises stress for primary loads in the central axis

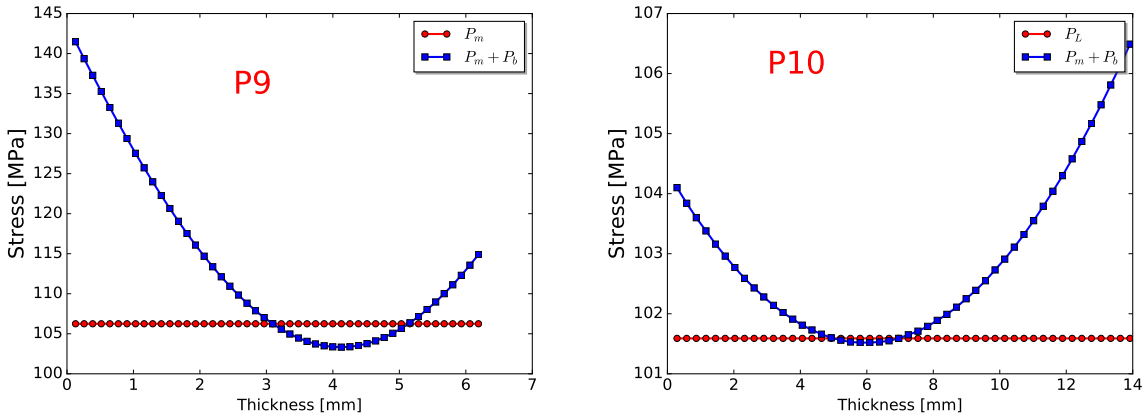

Figure 37: Equivalent Von Mises stress for primary loads in the central axis.

Primary and secondary loads

Figure 38 shown Von-Mises equivalent stress taking into account primary (DW+Pressure) and secondary loads (Temperature after the pulse, Figures 24 and 26). According to DPA analysis (Figure 15), only the PBEW and the final section of the shroud have to be consider as irradiated material (DPA above 2.5 dpa).

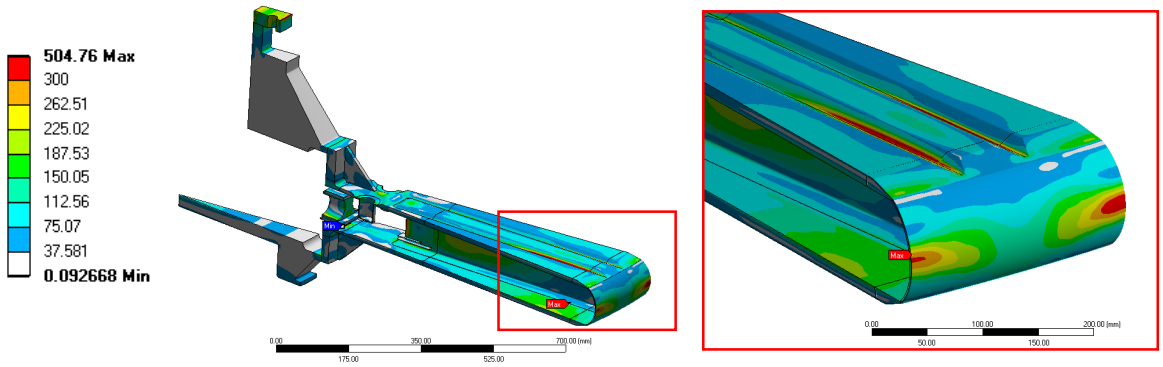

Figure 38: Equivalent Von Mises stress for secondary loads

The PBW have to withstand 3.6 dpa with a maximum temperature close to 300^oC. According to the design code, the limits are $S^A_{em} \sim 2214MPa$ and $S^A_{et} \sim 3861MPa$. Figure 40 shows the stress distribution in the PBW which clearly shows stress values almost a factor of 5 lower than the limits. The analysis of the linearized paths places in the welding position (Q1) and the PBW (Q2) confirms this safety factors. The stress values shown on the welding position are compatible with 0.5 welding coefficient which means that inspections are not needed to ensure the welding behavior. Nevertheless, surface inspection (visual and penetrant testing) and volumetric (radio test) will be included in the inspection plan.

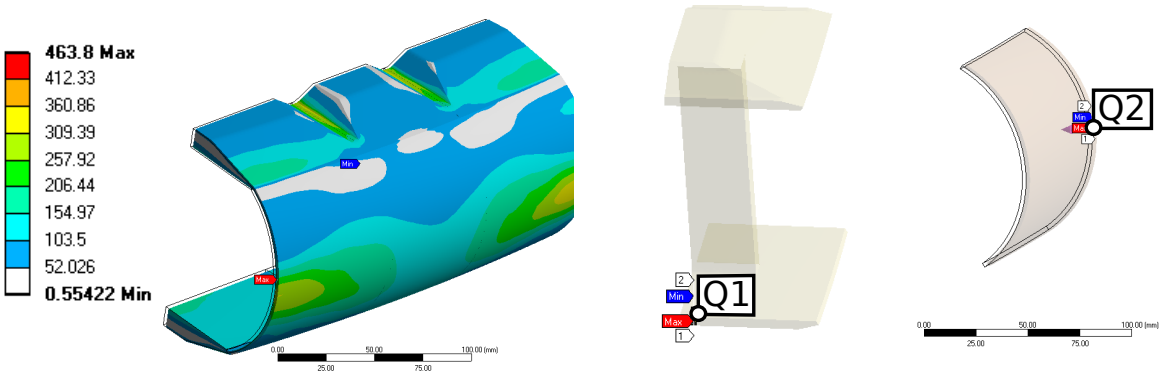

Figure 39: Equivalent Von Mises stress for secondary loads in the PBW

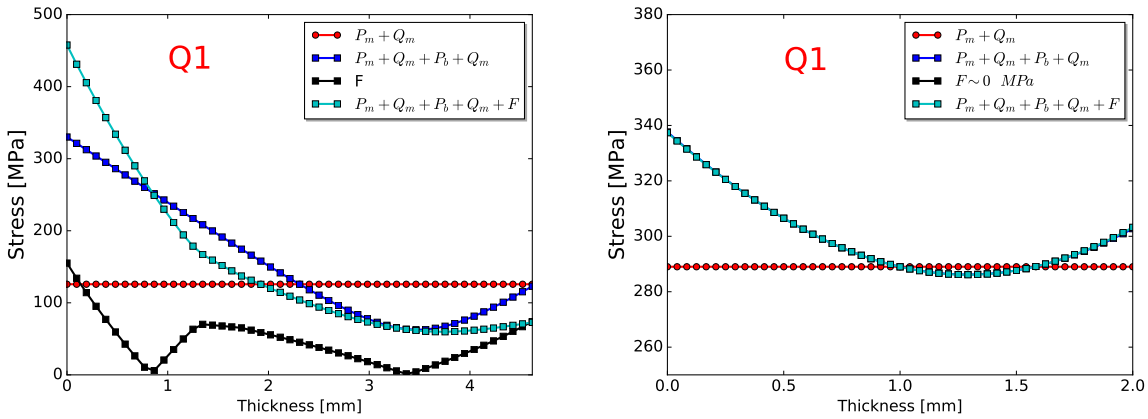

Figure 40: Equivalent Von Mises stress for secondary loads. Linearized paths Q1 and Q2 in PBW.

The Ribs section shows significant stresses in the thickness reduction as it is shown on Figure 41. Taking into account temperature ($< 200^oC$) and radiation damage ($< 3dpa$), the limits are $S^A_{em} \sim 3097MPa$ and $S^A_{et} \sim 5344MPa$. The Linearized analysis showed on Figure 42 shows negligible $P_m + Q_m$ values for both paths. Regarding the $P_m + Q_m + P_b + Q_b + F$ the maximum value is below 400 MPa more than a factor of 10 lower than S^A_{et}. Despite of the fact that peak stress can not be consider as complete solved, according to ASME rules the stress concentration will not increase the peak stress more that a factor of 4. Taking into account that the area is more that a factor of 10 lower than $S^A_{et} = 5344$ MPa no additional analysis is needed.

Finally the linearized path in the back of the Rib (Q4) shows only membrane stress and almost a factor of 10 lower than S^A_{em} an so, no additional analysis is required.

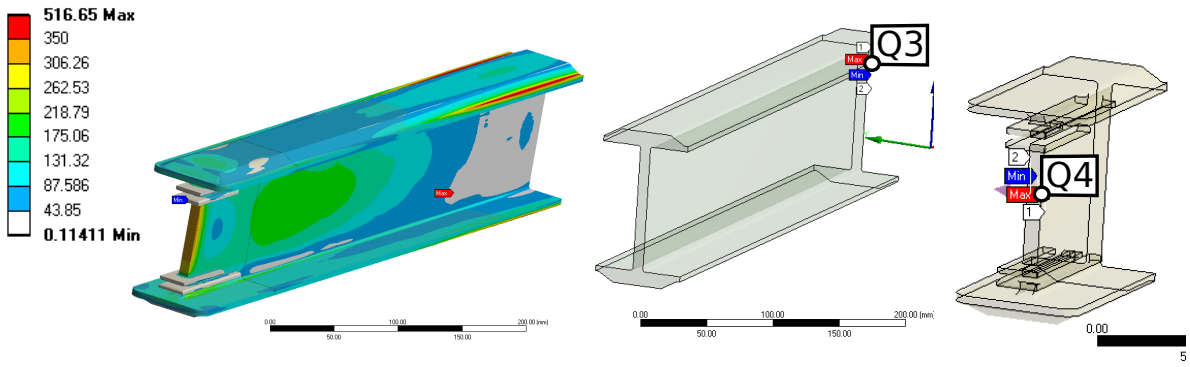

Figure 41: Equivalent Von Mises stress for secondary loads in the RIB.

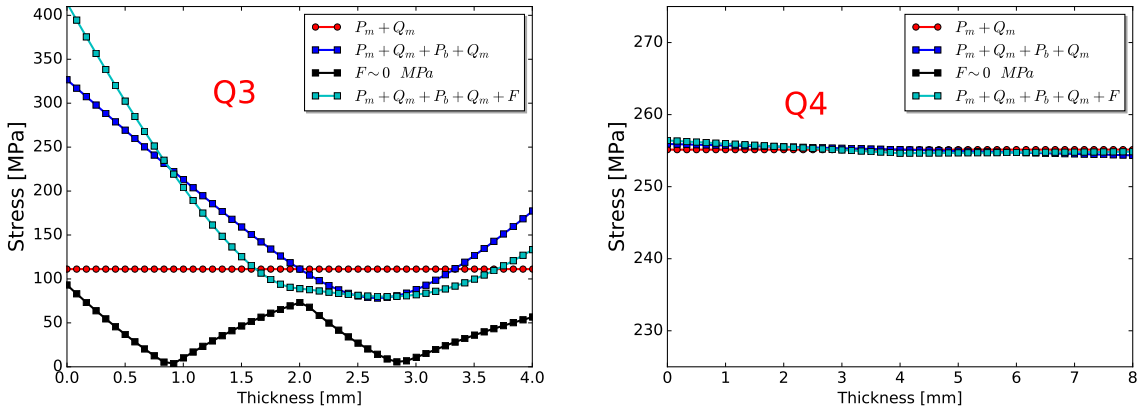

Figure 42: Equivalent Von Mises stress for secondary loads. Linearized paths Q3 and Q4

Finally the Axe stresses are shown on Figure 43. The radiation damage in this region can be consider negligible thus, no secondary loads analysis is needed according to the code. Nevertheless, the stress values are almost a factor of 5 lower that limits for not irradiated material.

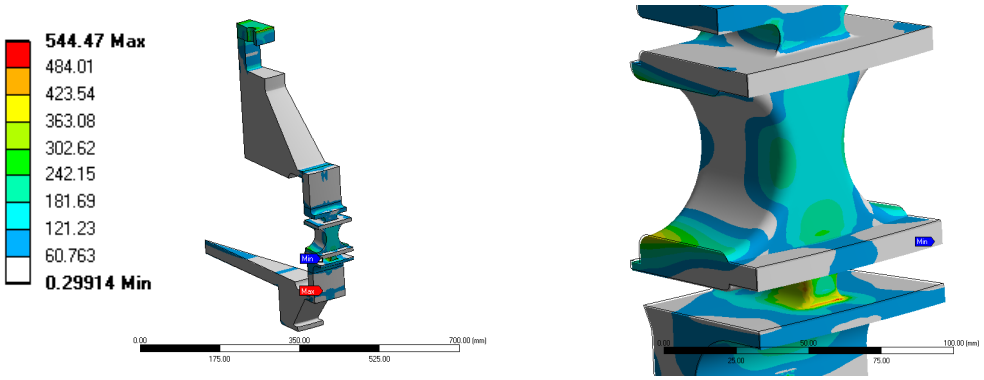

Figure 43: Equivalent Von Mises stress for secondary loads in the AXE.

8.2.4 Vertical displacement

The Target system is place at 20 mm from the moderator in order to maximize the neutron flux on it. The moderator is a very fragile that could be damage is the target clash on it. Figure 44 shows the maximum vertical deformation of the vessel in from of the moderator produced by primary loads ($\sim$ 0.6 mm). Ones the target arrives to steady state conditions the deformation increase to $\sim$ 1 mm. In both cases the deformation are relative low compare with the target to moderator gap.

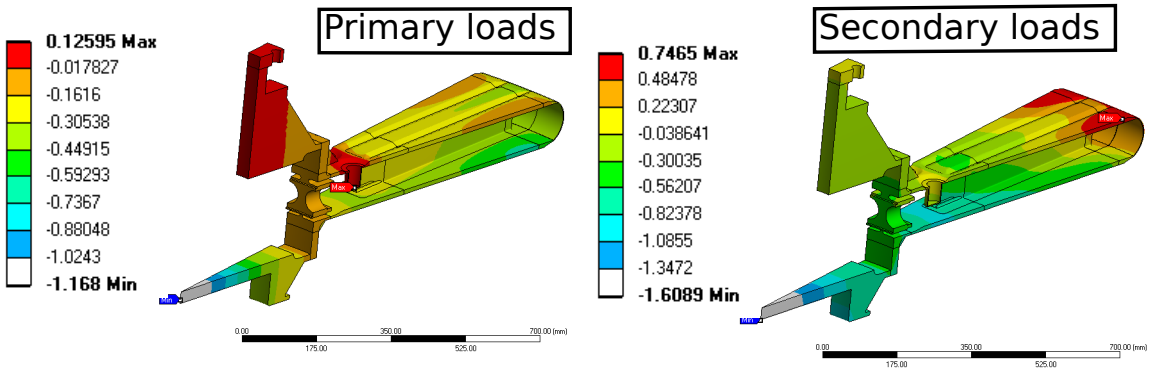

Figure 44: Directional (Z axis) deformation for primary and secondary loads.

S damage analysis (S1-SF2)

The TWV will suffer a significant amount of transients that can produce fatigue effects. This transients can be sumarized according to the specifications [30] as it is shown on Figure 45. This full stress history can be divided into different kind of stress:

- The stress range S_1 coming from the mass itself. This one is present along the full lifetime of the wheel.
- The stress range S_2 due to pressure and rotational velocity of the wheel. This one is coming back to 0 at each shutdown for maintenance of the facility.
- The stress range due to thermal loads produced by beam trips. The stress range is associated to the thermal gradient produced in the colling process, and this process is proportional to the length of the beam trip. The following has been identified:
  - S_3 coming from the time-average thermal load.
  - The stress S_5 due to beam trips of duration t: 2.4s $<$ t $<$ 10s.
  - The stress S_6 due to beam trips of duration t: 10s $<$ t $<$ 30s.
  - The stress S_7 due to beam trips of duration t: 30s $<$ t $<$ 60s.
  - The stress S_8 due to beam trips of duration t: 60s $<$ t $<$ 100s.
- The stress S_4 coming from shutdown.

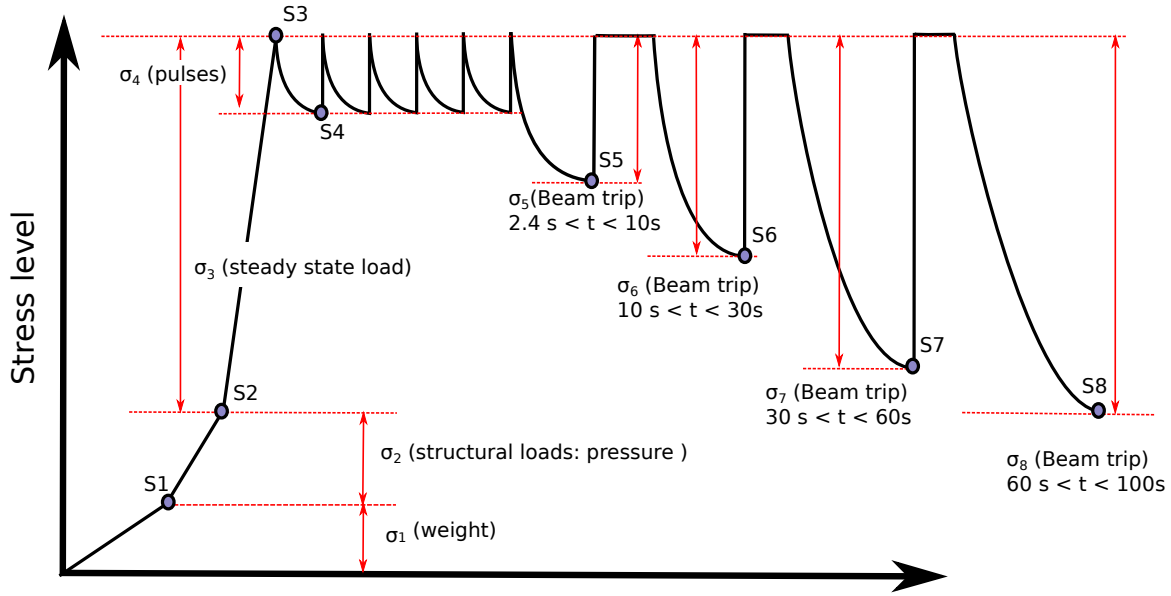

Figure 45: Cycles for the ESS Target

The table 8 shows the number of cycles associated to the different transients described on previous paragraphs. The maximum stresses achieved on each transient are produced in different sections of the target. Hence, the fatigue analysis will be divided on BPEW, Shroud and axis.

Event	Number	$\Delta\sigma_{thermal}$
S_1	1	–
S_2	175	–
S_3	8981	8981
S_4	4.6E+7	4.6E+7
S_5	39069	39069
S_6	31219	31219
S_7	26047	26047
S_8	21735	21735

Table 8: Number of occurrences per event

The temperature distribution corresponded to transient S2,S3 and S4 corresponds to the nominal conditions described on section 8.2.2. The temperature distribution for S5,S6,S7 and S8 are reproduced according to a cold down transient evaluated with the general CFD model [8] starting from temperature distribution of S3. Figures 46 and 50 and shows the temperatures achieved on the shroud and PBEW.

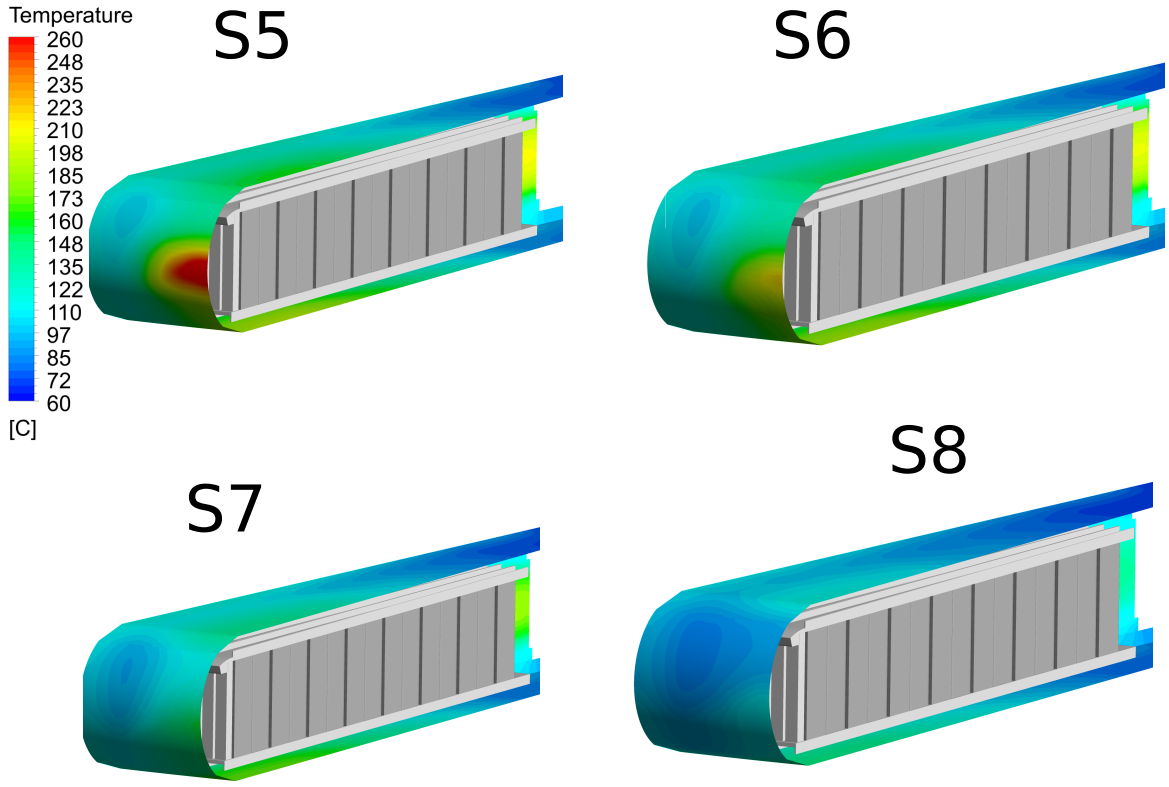

Figure 46: Shroud temperature distribution during the cold down. Temperatures evaluated by means of CFD model described on ESS-0066301 [8]

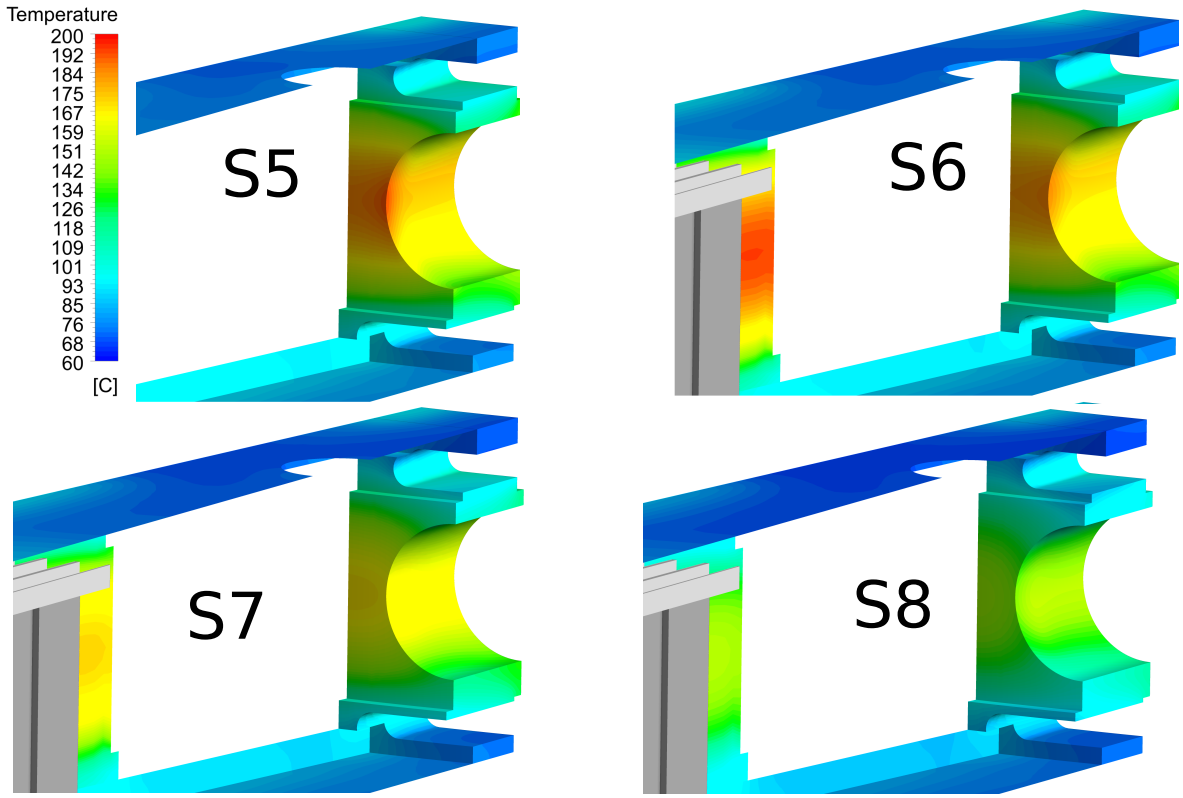

Figure 47: Axis temperature distribution during the cold down. Temperatures evaluated by means of CFD model described on ESS-0066301 [8]

PPBEW fatigue analysis

The PPBEW is exposed directly to the proton beam and so, all the transients produce significant stress amplitudes. The nominal operation (σ_4 produce temperature fluctuations in the PPBEW in the range of 20^oC and according to that, stresses far below the threshold to produce any fatigue effect.

The cold down produces a fast reduction of PPBEW temperature. This thermal gradient only generates appreciable fatigue effects for σ_7 and σ_8 which produces usages factors between 0.05 to 0.06.

Finally, the σ_3 produces an stress amplitude up to 410 MPa which can generate significant fatigue effects. However, the number of cycles is relative limited and the final usage factor do not exceeds 0.23. It should be remark that the maximum amplitude on transient σ_3 is not produced

in the same position as cold down transient at it is shown on Figure 49, based on that the analysis is conservative.

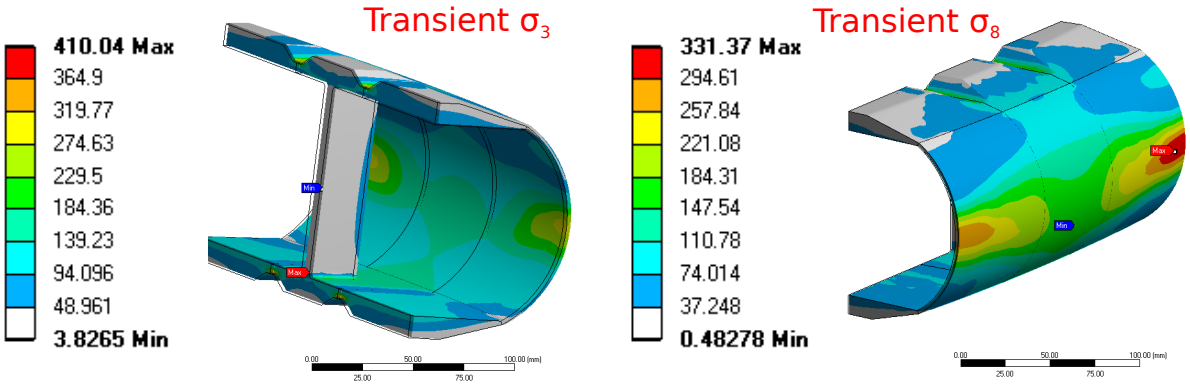

Figure 48: Stress amplitude in the PPBEW region for transients σ_3 and σ_8.

		σ_2	σ_3	σ_4	σ_5	σ_6	σ_7	σ_8
		S2	S3-S2	S3-S4	S3-S5	S3-S6	S3-S7	S3-S8
N		176	8,98E+03	3,50E+07	3,91E+04	3,12E+04	3,12E+04	2,17E+04
Temperatura	[ÂžC]	20	300	300	300	300	300	300
E	[Mpa]	1,76E+05	1,76E+05	1,76E+05	1,76E+05	1,76E+05	1,76E+05	1,76E+05
ν		0,3	0,3	0,3	0,3	0,3	0,3	0,3
$\Delta\sigma_{tot}$	[Mpa]	236	410	45	170	270	312	331
$\Delta(P\_m)$	[Mpa]	0	0	0	0	0	0	0
$\Delta(P\_b + P\_L)$	[Mpa]	22.5	0	0	0	0	0	0
$\Delta[0,33 * P_m + 0.67 * (P_b + P_L)]$	[Mpa]	106,50E+00	0,00E+00	0,00E+00	0,00E+00	0,00E+00	0,00E+00	0,00E+00
$K\varepsilon$		1,1524	1,1524	1,1524	1,1524	1,1524	1,1524	1,1524
K_v		1,098	1,098	1,098	1,098	1,098	1,098	1,098
$\Delta\varepsilon_1$ (%)		0,1162	0,2019	0,0222	0,0837	0,1330	0,1536	0,1630
$\Delta\varepsilon_2$ (%)		0,04	0,0000	0,0000	0,0000	0,0000	0,0000	0,0000
$\Delta\varepsilon_3$ (%)		0,0177	0,0308	0,0034	0,0128	0,0203	0,0234	0,0248
$\Delta\varepsilon_4$ (%)	0,0114	0,0198	0,0022	0,0082	0,0130	0,0151	0,0160	
$\Delta\varepsilon_t$ (%)	0,1841	0,2524	0,0277	0,1047	0,1662	0,1921	0,2038	
$\Delta\varepsilon_t$ (%)		0,3990	0,2671	0,1461	0,1461	0,1744	0,2094	0,2140
N		1,00E+04	4,00E+04	1,00E+08	1,00E+08	8,00E+06	5,00E+05	3,50E+05
VA		0,018	0,225	0,000	0,000	0,004	0,062	0,062
Va total	**0,371**							

Table 9: Fatigue analysis for PPBEW

Shroud fatigue analysis

The shroud is almost at constant temperature during the cooling transients because it is in contact with the inlet flow. As it can be shown on table 10 transients from σ_4 to σ_8 do not produce any stress amplitude above fatigue threshold.

Nevertheless, the transient σ_3 produces stresses amplitude in the range of 430 MPa in the welding line due to the thickness reduction. This stress value produces and usage factor of ~ 0.6 and hence, the area still have a significant safety factor. Taking into account the safety factors proposed by the code on welding lines, surface inspection and volumetric inspection will be needed.

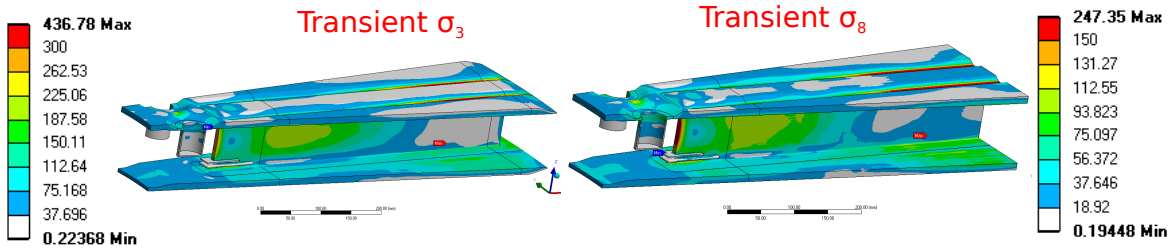

Figure 49: Stress amplitude in the Shroud region for transient σ_3 and σ_8.

		σ_2	σ_3	σ_4	σ_5	σ_6	σ_7	σ_8
		S2	S3-S2	S3-S4	S3-S5	S3-S6	S3-S7	S3-S8
N		176	8,98E+03	3,50E+07	3,91E+04	3,12E+04	2,60E+04	2,60E+04
Temperatura	[ÂžC]	30	130	130	130	120	120	100
E	[Mpa]	1,76E+05	1,76E+05	1,76E+05	1,76E+05	1,76E+05	1,76E+05	1,76E+05
ν		0,3	0,3	0,3	0,3	0,3	0,3	0,3
$\Delta\sigma_{tot}$	[Mpa]	450	430	5	103	97	143	250
$\Delta(P\_m)$	[Mpa]	23	0	0	0	0	0	0
$\Delta(P\_b + P\_L)$	[Mpa]	85	0	0	0	0	0	0
$\Delta[0,33 * P_m + 0.67 * (P_b + P_L)]$	[Mpa]	0,00E+00	0,00E+00	0,00E+00	0,00E+00	0,00E+00	0,00E+00	0,00E+00
$K\varepsilon$		1,34	1,34	1,34	1,34	1,34	1,34	1,34
K_v		1,18	1,18	1,18	1,18	1,18	1,18	1,18
$\Delta\varepsilon_1$ (%)		0,2216	0,2117	0,0025	0,0507	0,0478	0,0704	0,1231
$\Delta\varepsilon_2$ (%)		0,0331	0,0000	0,0000	0,0000	0,0000	0,0000	0,0000
$\Delta\varepsilon_3$ (%)		0,0763	0,0729	0,0008	0,0175	0,0165	0,0243	0,0424
$\Delta\varepsilon_4$ (%)		0,0410	0,0391	0,0005	0,0094	0,0088	0,0130	0,0228
$\Delta\varepsilon_t$ (%)		0,3720	0,3238	0,0038	0,0776	0,0730	0,1077	0,1883
$\Delta\varepsilon_t$ (%)		0,3974	0,3536	0,1576	0,1576	0,1583	0,1583	0,2071
N		1,00E+04	1,50E+04	1,00E+08	1,00E+08	1,00E+08	1,00E+08	3,00E+06
VA		0,018	0,599	0,000	0,000	0,000	0,000	0,009
Va total	**0,625**							

Table 10: Fatigue analysis for Shroud

Axis fatigue analysis

The stress amplitude produced in the axis region is driven by the outlet temperature. In the case of transient σ_4 and σ_5 and σ_6 outlet temperature is not significantly affected and according to that, the stress amplitude in the axis is relative low. The transients σ_7 and σ_8 produces significant reductions of outlet temperature and stress amplitude is appreciable (Figure 50). However, the total value ($\Delta[P_m + Q_m + P_b + Q_b + Peak]$) is below the threshold to produce fatigue in the material.

Regarding transitory σ_4, the stresses amplitude produced are close to 500 MPa and it could have a significant effect in fatigue. However, the number of cycles is relative low and the final usage factor is in 0.15. Based on this analysis we can conclude that fatigue is not expected in the axis region.

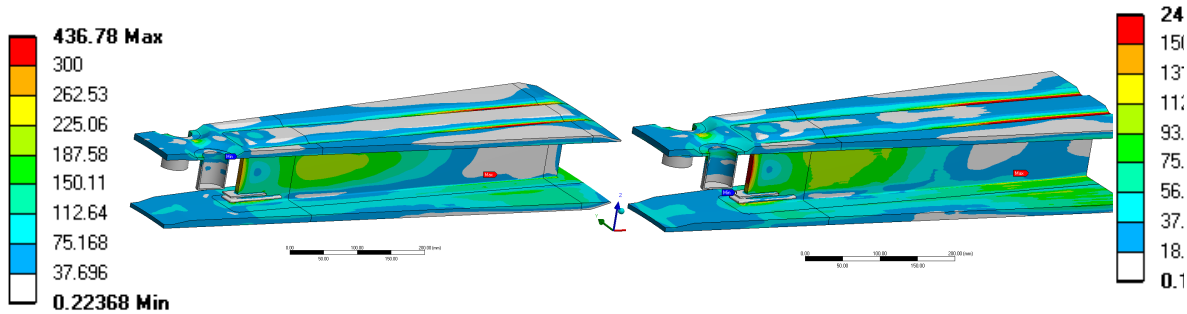

Figure 50: Stress amplitude in the axis region for transient σ_8.

		σ_2	σ_3	σ_4	σ_5	σ_6	σ_7	σ_8
		S2	S3-S2	S3-S4	S3-S5	S3-S6	S3-S7	S3-S8
N		176	8,98E+03	3,50E+07	3,91E+04	3,12E+04	2,60E+04	2,17E+04
Temperatura	[ÂžC]	30	140	140	140	130	115	100
E	[Mpa]	1,76E+05	1,76E+05	1,76E+05	1,76E+05	1,76E+05	1,76E+05	1,76E+05
ν		0,3	0,3	0,3	0,3	0,3	0,3	0,3
$\Delta\sigma_{tot}$	[Mpa]	320	475	1	101	93	135	205
$\Delta(P\_m)$	[Mpa]	31,8	0	0	0	0	0	0
$\Delta(P\_b + P\_L)$	[Mpa]	90,09	0	0	0	0	0	0
$\Delta[0,33 * P_m + 0.67 * (P_b + P_L)]$	[Mpa]	7,09E+01	0,00E+00	0,00E+00	0,00E+00	0,00E+00	0,00E+00	0,00E+00
K_ε		1,23	1,23	1,23	1,23	1,23	1,23	1,23
K_v		1,14	1,14	1,14	1,14	1,14	1,14	1,14
$\Delta\varepsilon_1$ (%)		0,1576	0,2339	0,0005	0,0497	0,0458	0,0665	0,1009
$\Delta\varepsilon_2$ (%)		0,0349	0,0000	0,0000	0,0000	0,0000	0,0000	0,0000
$\Delta\varepsilon_3$ (%)		0,0358	0,0532	0,0001	0,0113	0,0104	0,0151	0,0229
$\Delta\varepsilon_4$ (%)		0,0217	0,0322	0,0001	0,0068	0,0063	0,0092	0,0139
$\Delta\varepsilon_t$ (%)		0,2151	0,3193	0,0007	0,0679	0,0625	0,0907	0,1378
$\Delta\varepsilon_t$ (%)		0,2295	0,2757	0,1569	0,1569	0,1576	0,1586	0,1596
N		7,50E+05	6,00E+04	1,00E+08	1,00E+08	1,00E+08	1,00E+08	1,00E+08
V_a		2,3E-4	0,15	0,00000	0,00000	0,00000	0,00000	0,00000
Va total	**0,149918**							

Table 11: Fatigue analysis for Axis

8.3 SF2: Vertical displacement beam (1 cm)

The loads on this accidental scenario are produced by the design beam under nominal frequency, with the wheel at his nominal rotation speed. Also the beam is considered synchronized with the wheel and hitting the SS and tungsten with a positive vertical displacement of 1 cm from the center of the PBEW and the cassette, as indicated in Figure 51. The cooling system is working at nominal conditions, so helium mass flow trough the wheel is 2.85 kg/s which means 0.0792 kg/s in each cassette.

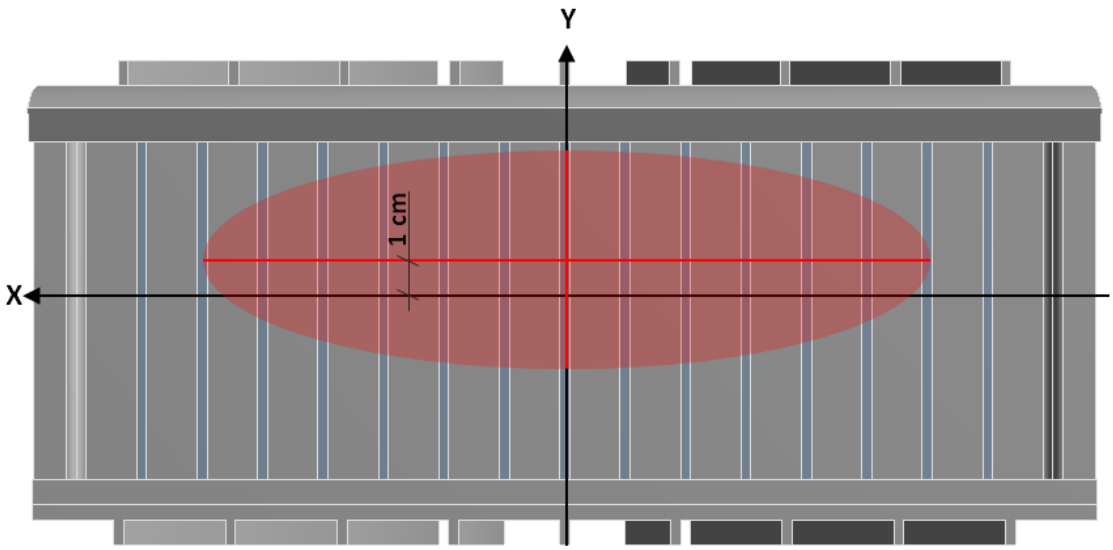

Figure 51: Beam vertical displacement

Temperature distribution

Figure 52 shows the maximum temperature of the different areas of the target for this accidental scenario. The vertical displacement of the beam moves the point of maximum heat load in the PBEW to an area with higher coolant velocity. The increase of the local velocity of the coolant produces higher heat transfer coefficient and thus a reduction of the maximum temperature in the PBEW window compared with the nominal conditions (Figure 53).

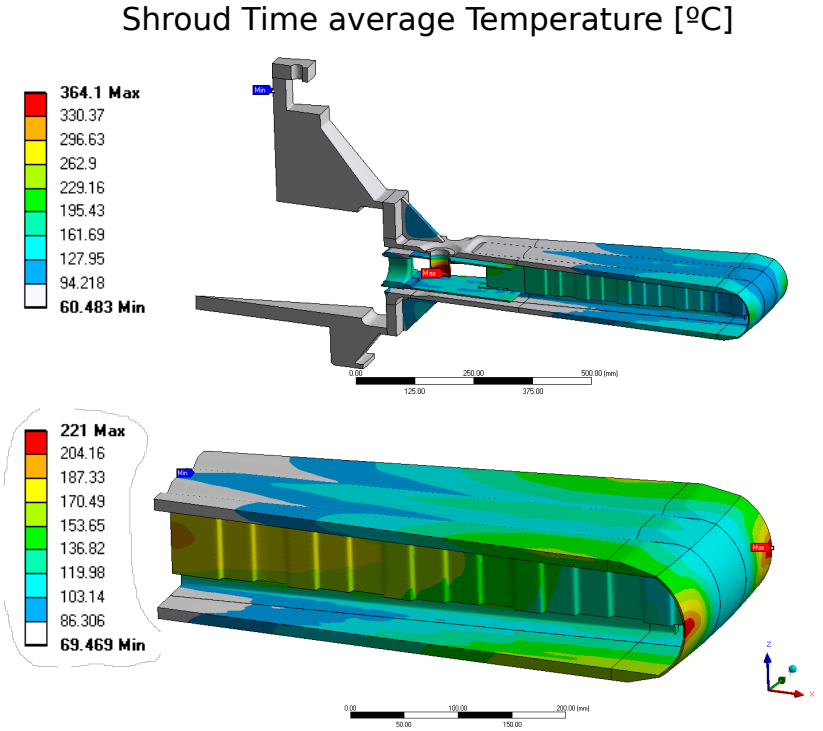

Figure 52: Temperature profile during the vertical displacement beam (1 cm) scenario.

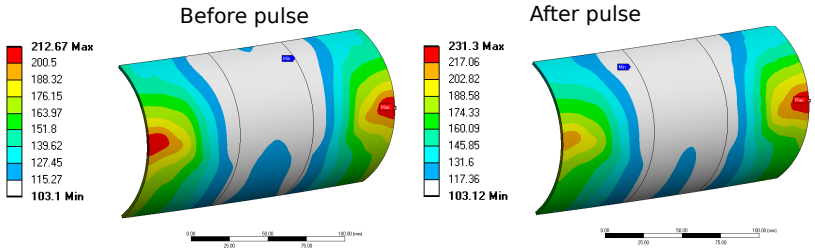

Figure 53: Temperature profile in the PBEW during the vertical displacement beam (1 cm) scenario.

P damage analysis

The analysis for P damage is based on the FEM mechanical model described on section 5.4 considering elastic properties for materials. Primary loads are produced by dead weights and the difference pressure between internal pressure and monolith vessel vacuum (12 bar(g)). Regarding secondary loads, the temperature distribution shown on previous section (after the pulse) is

considered.

Primary loads

The analysis for primary loads is analogous to Section 8.2.3 so, no additional analysis is needed.

Secondary loads

The maximum temperature on the BEW at steady state conditions will not produce the temperature failure of the component, however, the PBEW is an irradiated area hence, secondary stresses have to be consider according to $RCC-MR_x$ design code. Figure 54 shows the Equivalent Von Mises stress for primary and secondary loads considering steady state conditions.

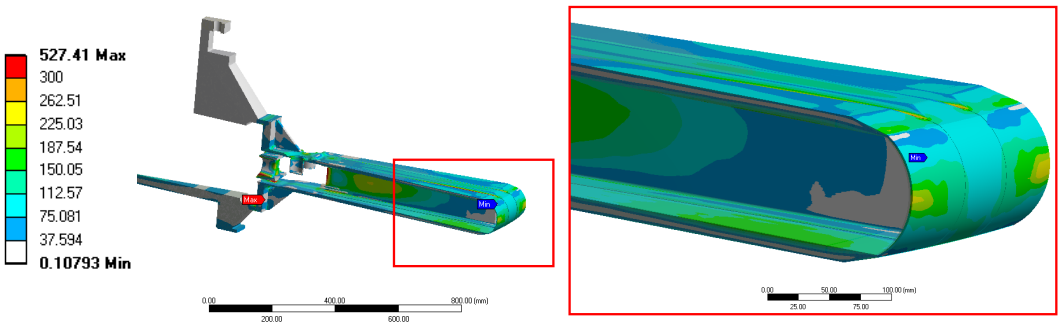

Figure 54: Equivalent Von-Mises stress during the vertical displacement beam (1 cm) scenario.

Figures 55 and 56 shows the stress distribution in the PBEW. The analysis of the linearized paths shows membrane stresses ($P_m + S_m$) between 100-200 MPa, more than a factor of 10 lower than the limits proposed by the code. Regarding total stresses ($P_m + Q_m + P_b + Q_b + F$) the safety factor is similar hence, no additional analysis is needed.

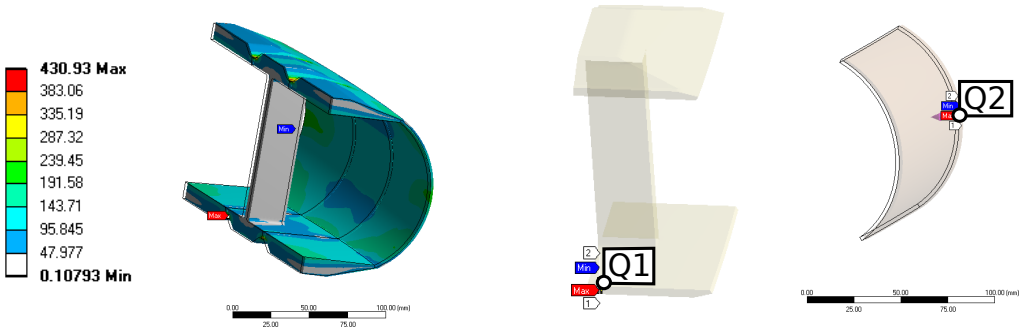

Figure 55: Equivalent Von-Mises stress during the vertical displacement beam (1 cm) scenario on PBEW.

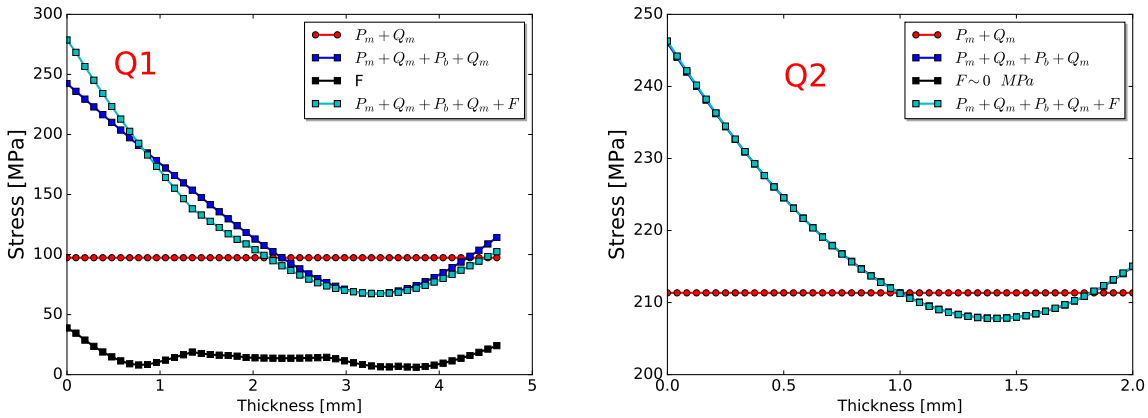

Figure 56: Linearized analysis for primary and secondary loads during the vertical displacement beam (1 cm) scenario. Linearized paths position showed on Figure 55

The Ribs section shows significant stresses in the thickness reduction as it is shown on Figure 57. Taking into account temperature ($< 200^oC$) and radiation damage ($< 3dpa$), the limits are $S^A_{em} \sim 3097MPa$ and $S^A_{et} \sim 5344MPa$. The Linearized analysis showed on Figure 58 shows low $P_m + Q_m$ values for both paths. Regarding the $P_m + Q_m + P_b + Q_b + F$ the maximum value is below 460 MPa more than a factor of 10 lower than S^A_{et}. Despite of the fact that peak stress can not be consider as complete solved, according to ASME rules the stress concentration will not increase the peak stress more that a factor of 4. Taking into account that the area is more that a factor of 10 lower than $S^A_{et} = 5344$ MPa no additional analysis is needed.

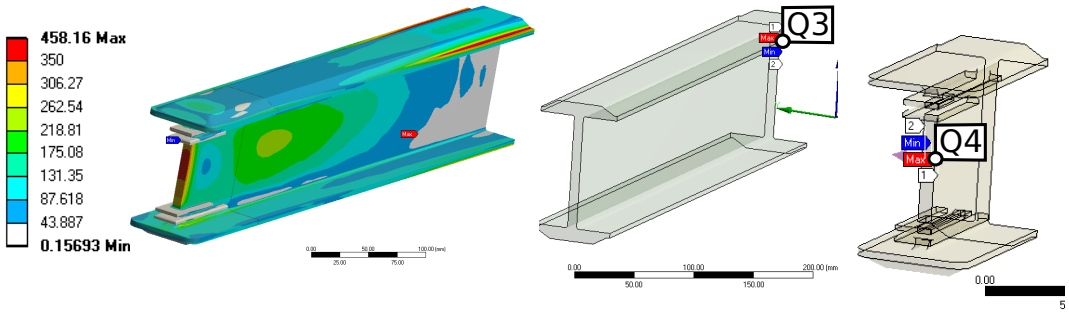

Figure 57: Equivalent Von-Mises stress during the vertical displacement beam (1 cm) scenario on RIB.

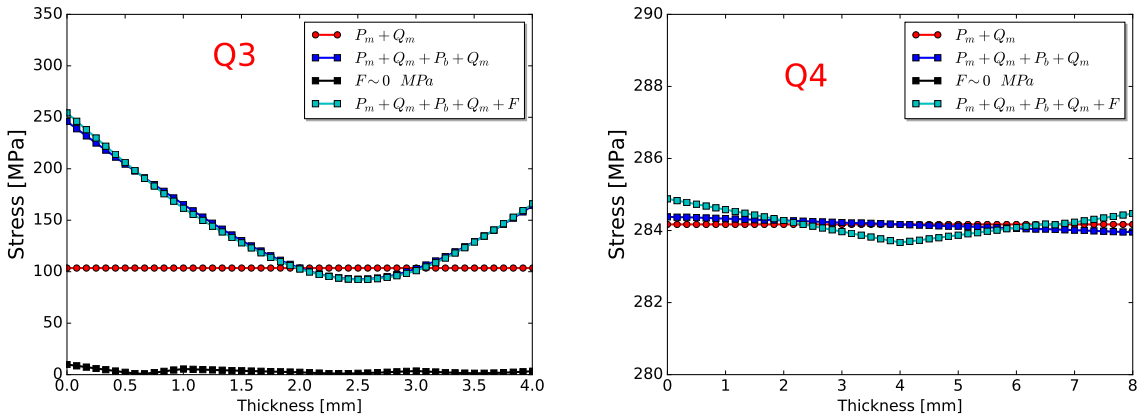

Figure 58: Linearized analysis for primary and secondary loads during the vertical displacement beam (1 cm) scenario. Linearized paths position showed on Figure 57

Finally the Axe stress is shown on Figure 59. The radiation damage in this region can be consider negligible thus, no secondary loads analysis is needed according to the code. Nevertheless, the stress values are almost a factor of 5 lower that limits for not irradiated material.

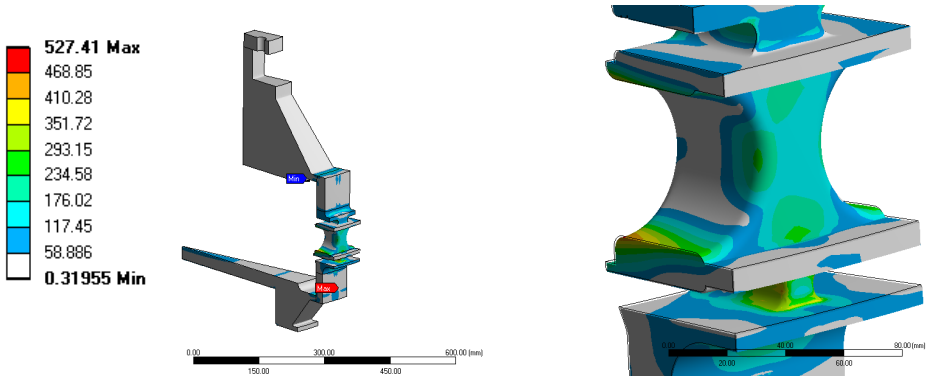

Figure 59: Equivalent Von Mises stress during the vertical displacement beam (1 cm) scenario on AXE.

8.4 SF2 Wheel-Beam desynchronization

8.4.1 Heat load

In this section the Target Vessel thermo-mechanical results are presented for the SF2 Wheel-Beam desynchronization load scenario. In order to calculate the thermal load for this scenario, the model for nominal conditions is modified by rotating the wheel 5 degrees, using transformation cards in the MCNPX model. Notice that, since only 1 sector is fully detailed, symmetry conditions are used to get a full heat load. Figure 60 depicts the model used.

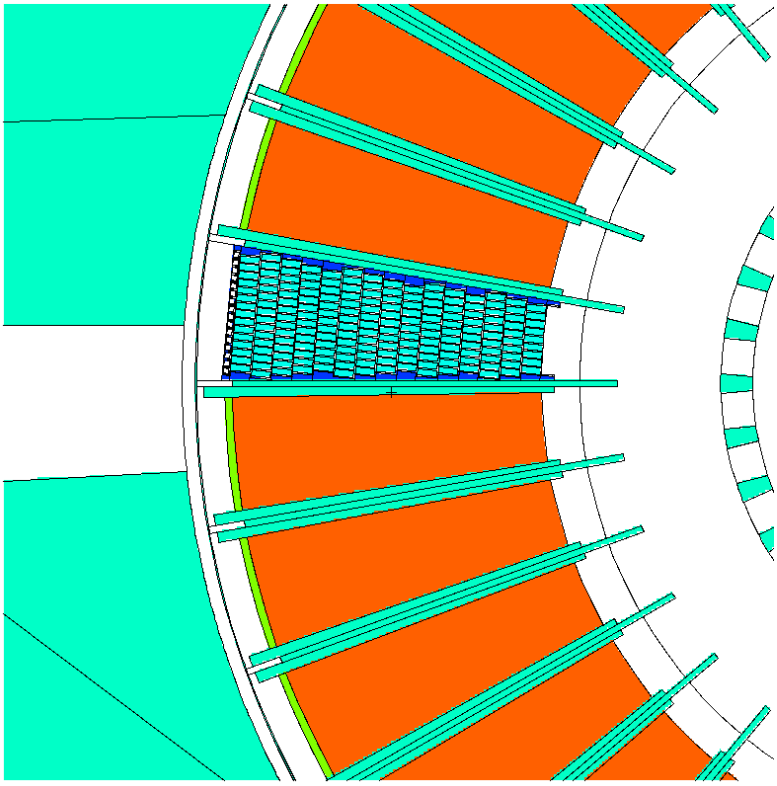

Figure 60: MCNPX Model for the SF2 scenario

In this accidental scenario, there is not really a single active sector, as the beam is hitting the area just between two of them. For the purposes of power tallying, we consider the two sectors next to the rib hit as 'active sector', in Table 12.

Zones	Max Power Density (W/cm3) t-aver		Power deposition (kW) t-aver	
	MCNP	CFD	MCNP	CFD
Tungsten	129.5	128.0	2085.4	2074.7
BEW	36.8	40.6	13.3	13.2
Cassette down	4.2	6.8	28.3	28.3
Cassette side	71.8	79.7	442.2	442.7
Cassette up	4.3	7.1	32.7	32.7
Shroud up	3.0	4.4	73.0	72.5
Shroud down	2.8	4.0	64.3	64.2
Rib	60.8	60.8	221.9	221.3
Cylinder	0.9	0.9	-	5.5
Separators	1.0	0.9	-	4.7
Dummies	85.2	45.5	-	13.8
		TOTAL	2961.1	2973.6

Table 12: Heat load in SF2 Wheel-Beam desynchronization scenario

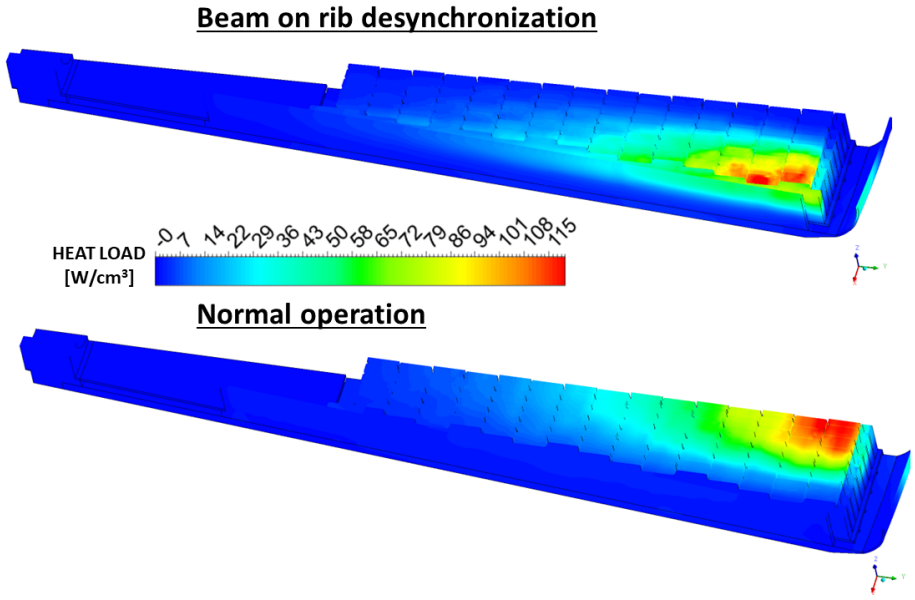

Figure 61: SF2 Wheel-Beam desynchronization and SF1 nominal operation load scenarios power density profiles

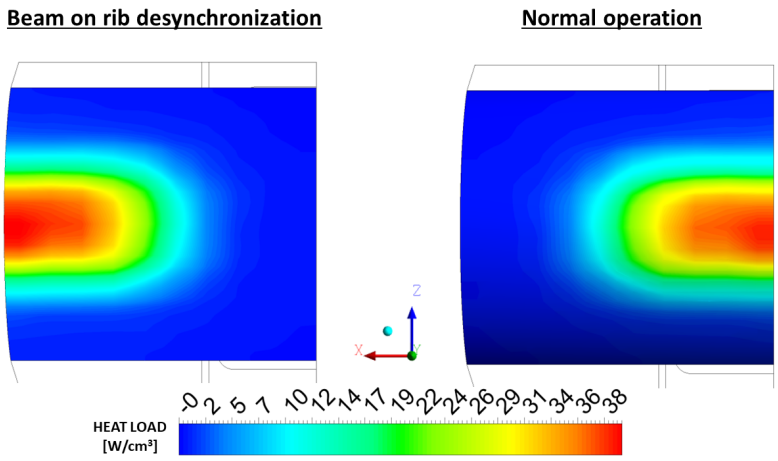

Figure 62: SF2 Wheel-Beam desynchronization and SF1 nominal operation load scenarios power density profiles in the beam entrance window.

8.4.2 CFD thermal analysis

The Target Vessel maximum temperature evolution during the accidental scenario is shown in Figure 63. CFD vessel sub-model 2 described on the document ESS-0066301 [8] was employed following the methodology detailed in section 5.7 to obtain the thermal results. The manufacturing path including calibrated plates adjustment [34] ensures gabs between rib and cassette lower than 0.05 mm hence, good contact between cassette and rib is considered (U=25000 W/m^2K).

The SS-316L mechanical limits according to RCC-MRx are temperature dependent which means the higher the operating temperature the lower the membrane and bending stress limits. Above 550 ^oC there are no defined limits so the vessel failure is assumed beyond this point.

From the transient simulation at average power (Step 2 on section 5.7), the temperature evolution during the desynchronization scenario is obtained. Figures 64 shows the temperature evolution for different areas of the Target wheel. The following considerations can be remarked:

- The spallation material maximum temperature is reduced during the first 10 s. After this point the maximum temperature increases up to overlap the maximum operational temperature.
- RIB temperature increases continuously and it achieves the 500^oC after 35 s.
- Shroud temperature decreases because its heat load is reduced.
- PBEW is not affected and the steady state maximum temperature will be similar to maximum nominal temperature.

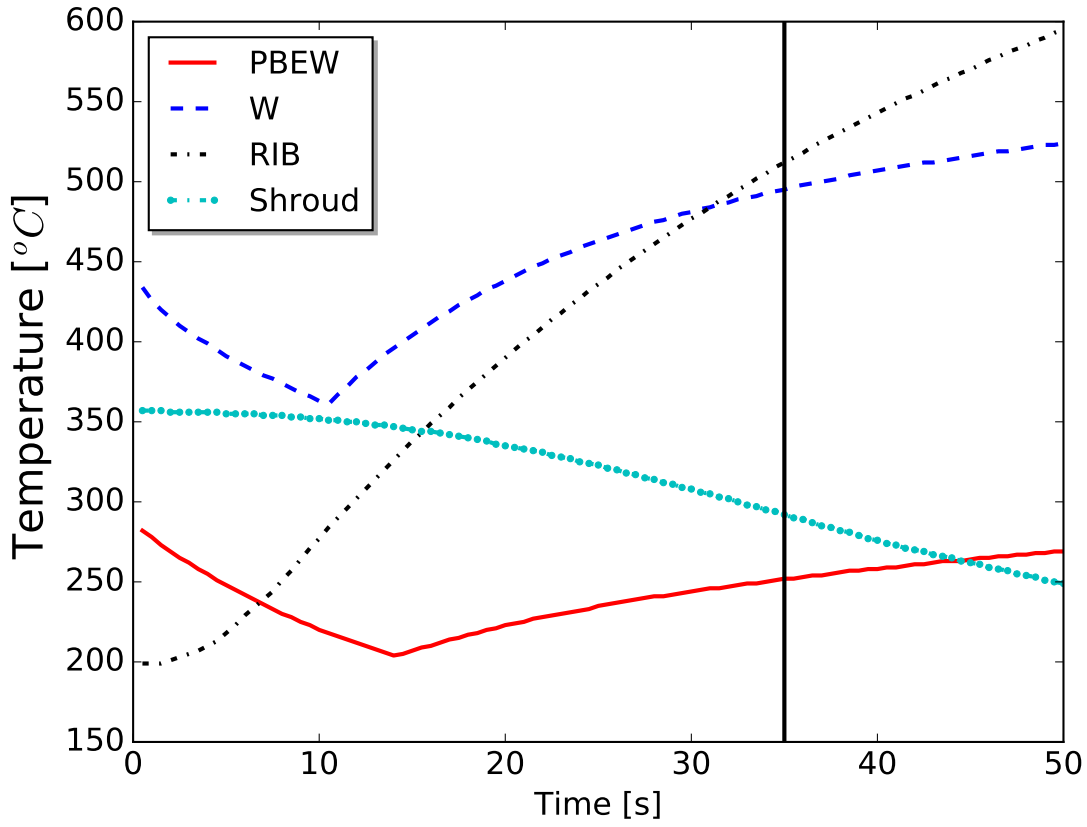

Figure 63: Vessel Rib and Cassette maximum temperature evolution during the SF2 Wheel-Beam desynchronization for different thermal contact configurations.

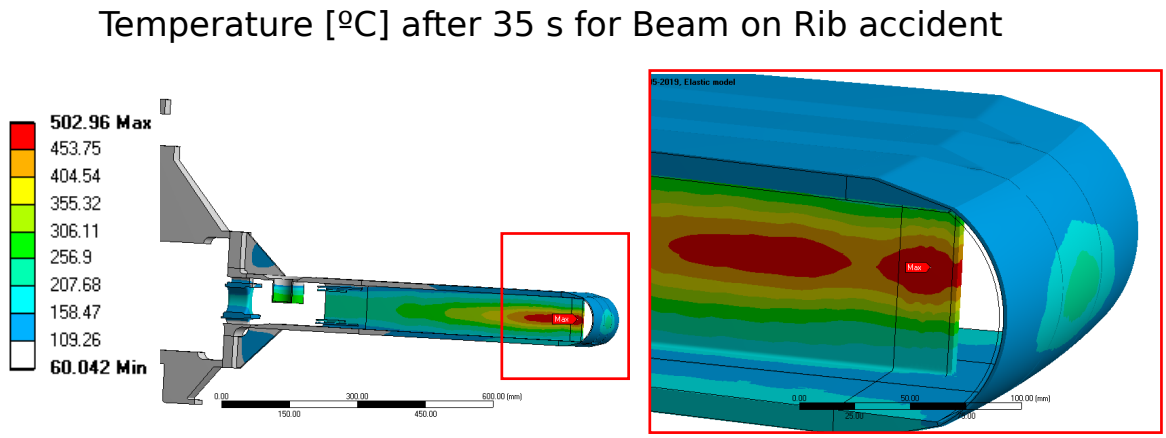

Figure 64: Maximum temperature during the SF2 Wheel-Beam desynchronization after 35 s.

8.4.3 Mechanical verification

According to previous section, the Rib achieves 500^oC after 35 s. Figure 65 shows secondary loads stress distribution according to temperature showed on Figure 64. The maximum stress is achieved in the external section of the Rib in which most of the stress can be consider as membrane ($P_m + Q_m$) and no bending stress is shown.

In order to evaluate the mechanical properties of the material, we will consider that the operation of the wheel has been produced mainly under operational conditions and so, the radiation damage distribution showed on Section 6 is still valid. According to this analysis, the maximum damage in the rib will be $\sim$ 1.1 dpa.

The value shown on Figure 66 is far below the mechanical limit proposed by the code under the rib temperature and radiation conditions ($S^A_{em}(< 2.75dpa, < 550C) = 1957$) hence, no mechanical failure will be produced.

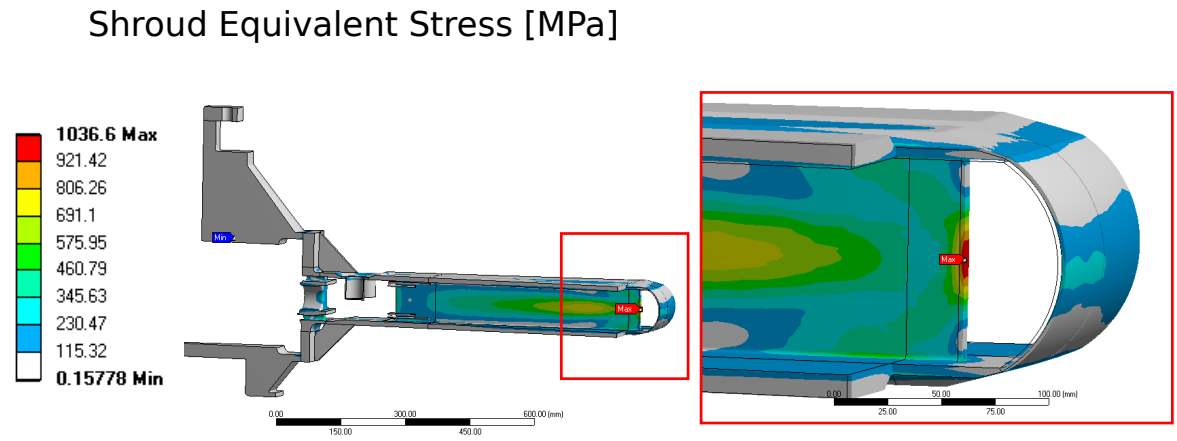

Figure 65: Maximum temperature during the SF2 Wheel-Beam desynchronization after 35 s.

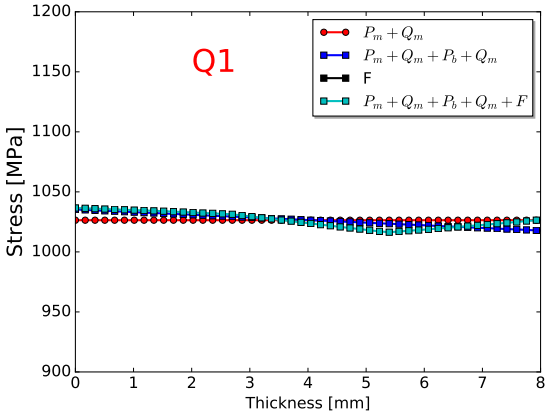

Figure 66: Linearized analysis for maximum stress region in the rib after 35 s for Wheel-Beam desynchronization event.

8.4.4 Conclusion for beam desynchronization

According to previous section, the failure of the vessel will be produced by the maximum temperature and no by mechanical stress. Based on the beam frequency on each rib, the temperature of 500^oC will be achieved after 14 pulses (35 s) which can be consider the operational limit for this scenario.

8.5 SF2: Shutdown

The shutdown scenario (Section 2) reproduces an accidental condition in which the beam is off and the helium cooling stops. In this situation the residual heat evaluated on section 7 have to be removed by radiation through the surrounded structures.

Several scenarios have been address based on the model described on Section 5.6. The evolution of maximum temperature is shown on Figures 67 and 68.

The reference scenario considers a Target Vessel emissivity (ϵ_{TV})of 0.6, shielding at 22^oC (T_{TV}) with an emissivity of 1.0 (ϵ_{SH}). On this conditions, the maximum temperatures of the Target is in the range of 320^oC.

However, the shielding that surrounds the Target vessel will increase its temperature unless active cooling continue working. There are several cases (blackout) in which this condition will not be fulfill. On the other hand, the shielding is mainly machined stainless steel in order to achieve the vacuum requirements in surface roughness [28]. The experiments carried out by UPV[27] shows emissivity values in the range of 0.3 if additional surface conditioning process is not performed. This second scenario ($\epsilon_{TV} = 1.0; \epsilon_{SH} = 0.3 : T_{SH} = 200^oC$) shows maximum temperatures close to 440^oC.

The third scenario evaluate shows the temperatures is the emissivity of the Target is reduced to 0.3. In this cases maximum temperatures are close to 475^oC. Finally, the scenario ($\epsilon_{TV} = 1.0; \epsilon_{SH} = 0.3 : T_{SH} = 200^oC$)* evaluates the temperature in case to gab between top cover and cassette is filled with air. This situation could be produced if there is a leak in the target and the maximum temperature is still below 500^oC.

Taking into account that the target fulfill the Design conditions (500^oC and 13 bar(g)) it can be consider that this accident is safe if the maximum temperature is below 500^oC. The scenarios associated to $\epsilon_{TV} = 0.3$ shows temperature close to 500^oC hence, it is recommended treat the target surface to increase the emissivity. As it will be described on manufacturing plan, the target external surface will be sandblasting to achieve surface roughness higher that $R_a \sim 4\mu m$ in order to ensure emissivity values higher than 0.5 at 400^oC.

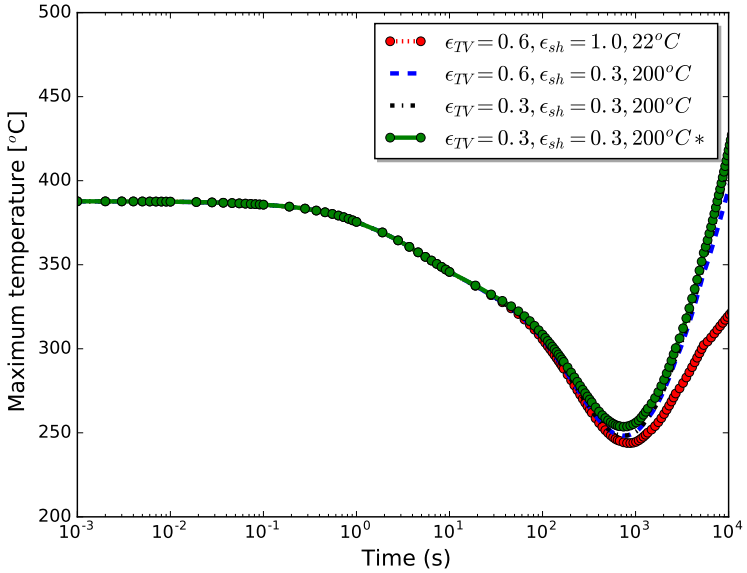

Figure 67: Maximum temperature of the Target for shutdown scenario

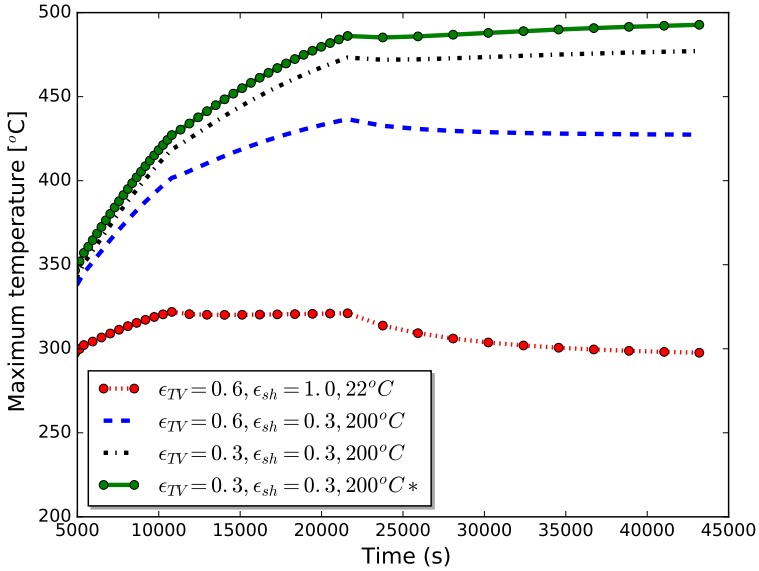

Figure 68: Maximum temperature of the Target for shutdown scenario

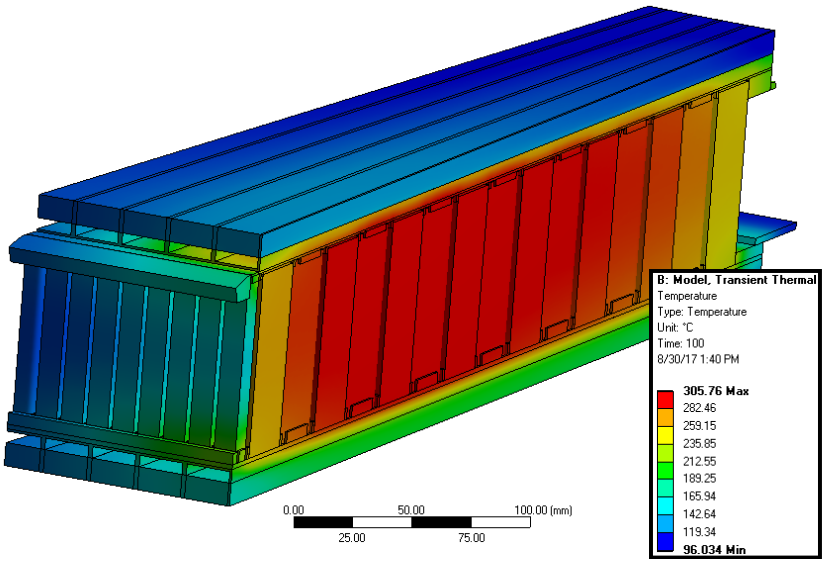

Figure 69: Temperature distribution for shutdown scenario after 100s. ($\epsilon_{TV} = 0.6$;$\epsilon_{SH} = 0.3$; T_{TV})

8.6 SF2: Loss of cooling

The reduction of cooling in the target will produces an increase of operational temperature of the shroud and if it exceeds the design temperature (500^oC) the failure of the TWV can be produced. Based on this hypothesis, thermal analysis will be perform to evaluate these accidental conditions.

The mass flow reduction is an scenario in which inlet flow is reduced keeping inlet temperature and pressure. The analysis is performed with the CFD model described on [8] and reducing inlet mass flows. Table 13 shows the maximum temperature of the different elements of the system related with mass flow reduction. Based on maximum temperature of the shroud, the Target Vessel will be below design conditions even at 80% of mass flow. Regarding thermal stresses, secondary loads will be far from $RCC - MR_x$ in all the cases.

Hence, from mechanical verification point of view, the shroud will survive to mass flow reductions without exceeds the protection level A criteria. However, the temperature of the spallation material will achieve peak temperatures close to 600^oC for mass flows lower than 2.23 kgs^{-1}.

	m	W	Rib	BEW	Shroud	Termometers
95%	2.70 kgs^{-1}	465^oC	210 ^oC 580 MPa	298 ^oC 355 MPa	202 ^oC 440 MPa	375 ^oC 263 MPa
90%	2.56 kgs^{-1}	481 ^oC	215 ^oC 580 MPa	309 ^oC 380 MPa	209 ^oC 580 MPa	390 ^oC 280 MPa
80%	2.23 kgs^{-1}	540 ^oC	241 ^oC 710 MPa	346 ^oC 560 MPa	244 ^oC 410 MPa	437 ^oC 320 MPa

Table 13: Maximum temperature for mass flow reduction

8.7 SF3: Unrastered-nominal beam

The thermal source obtained from MCMPX and used as input for the CFD analysis for the unrastered and nominal beam accidental scenario is shown in the figure 70. The maximum power density deposited during this accident scenario in the in the BEW and tungsten is approximately eight times higher than during normal operation.

Before the magnets failure which causes the lost of the beam raster, the maximum average temperature at normal operation (steady state analysis) of the tungsten, BEW and the cassette is 445 °C, 354 °C and 286.3 °C respectively. After the failure the maximum power density in the tungsten increases from $1.05 \cdot 10^8$ W/m^3 to $8.45 \cdot 10^8$ W/m^3 which produces a maximum temperature of 965 °C once reached again the steady state. The heat deposition in the BEW increases from $3.51 \cdot 10^7$ W/m^3 to $2.78 \cdot 10^8$ W/m^3 as consequence the BEW maximum temperature achieves 585 °C.

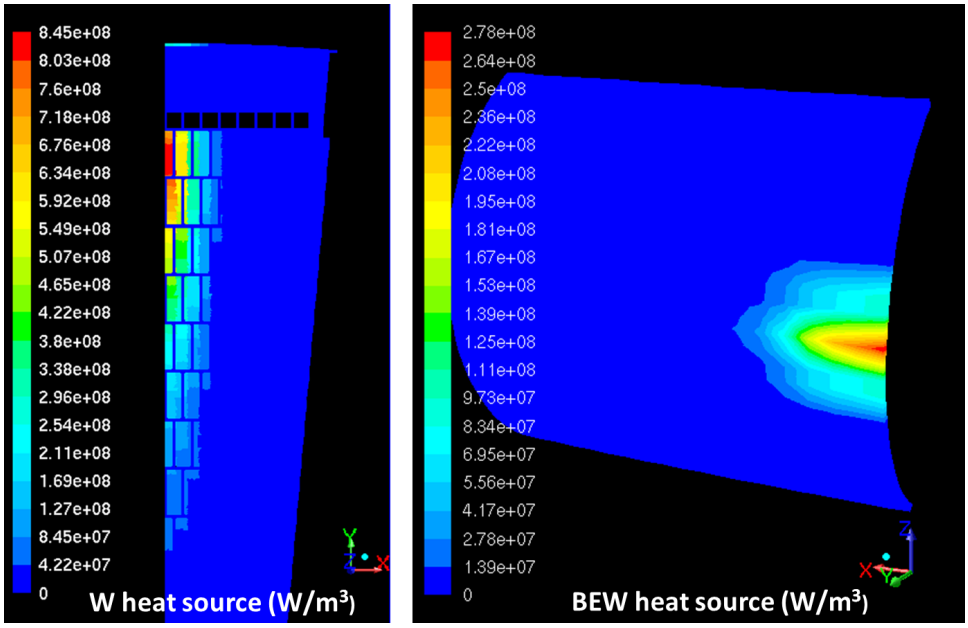

Figure 70: Thermal source at average current generated in the spallation material an the BEW by the unrastered and nominal beam

Figure 71 shows the maximum temperature of the different areas of the target vessel when steady state is achieved. The temperature of the PBEW is relative hight but considering that this transient will be limited in time it can be considered below the negligible creep line and thus acceptable (< 1 h). There is a also a lightly increase of shroud temperature due to the heat transfer through the cassette but, due to its low thermal conductivity the effect is not relevant.

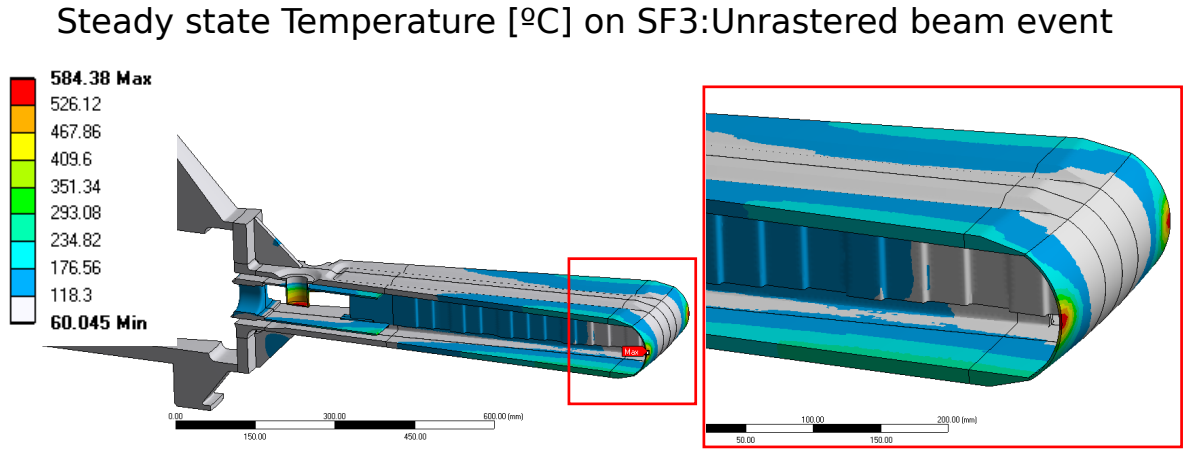

Figure 71: Maximum temperature evolution in the spallation material, BEW, cassette and number of bricks above 700 °C for a unrastered and nominal beam

Regarding secondary loads mechanical stresses, Figure 72 shows the equivalent stress distribution. As it was expected, the shroud and axis are not significantly affected by the heat load concentration. However, the PBEW shows a large increase on equivalent stress as it is shown on Figure 73. The linearized analysis shows that most of the stress is mainly $P_m + Q_m$ and it achieves 525 MPa however, it is still almost a factor of 2 below the S^A_{em} limit at 3.75 dpa and 550^oC ($\sim$ 1134 MPa). Regarding $P_m + Q_m + P_b + Q_b$ the maximum value is almost a factor 3 lower than the limit ($P_m + Q_m + P_b + Q_b \sim 775$ MPa $< S^A_{et} = 2101$ MPa).

Considering the large safety factor showed on secondary stress analysis and the absence of creep effects, we can consider that the target can withstand the accidental conditions under the protection level A.

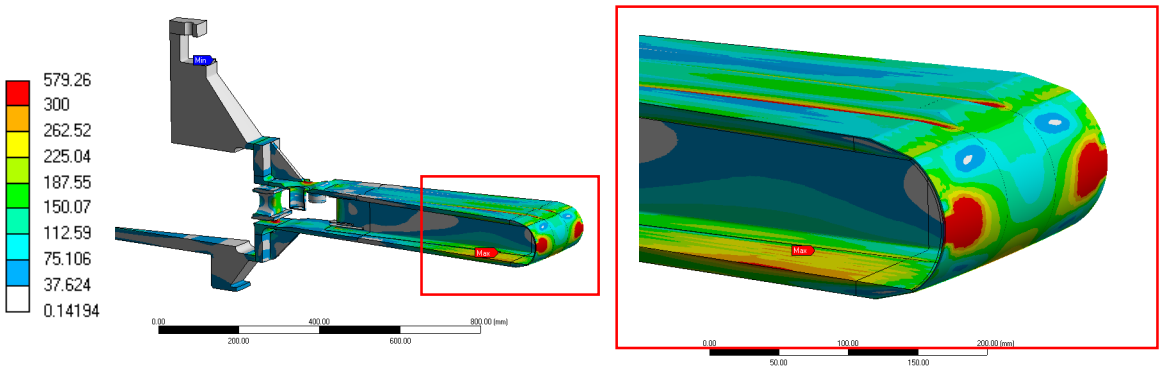

Figure 72: Von Misses equivalent stress for steady state conditions on Unrastered-nominal beam.

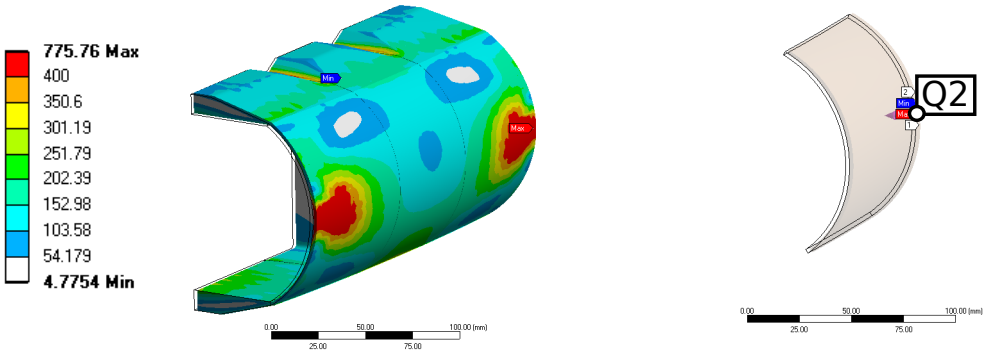

Figure 73: PBEW Von Misses equivalent stress for steady state conditions on Unrastered-nominal beam.

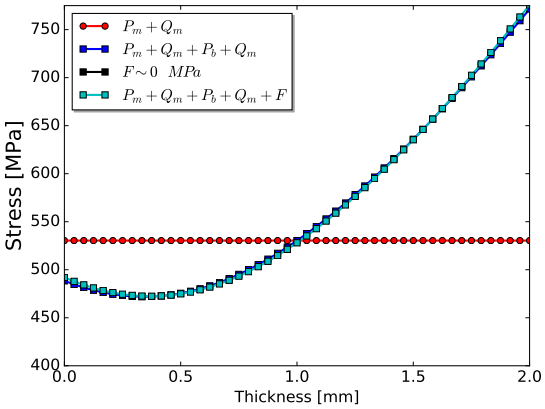

Figure 74: PBEW linearized equivalent Von Misses analysis on path Q2 showed on Figure 73.

8.8 SF3- Rastered-focused beam

The thermal source obtained from MCMPX and used as input for the CFD analysis for the rastered focused beam accidental scenario is shown in the figure 75. The maximum power density deposited during this accident scenario in the in the BEW and tungsten is approximately the same as for normal operation.

Before the magnets failure which causes the focus of the beam, the maximum average temperature at normal operation (steady state analysis) of the tungsten, PBEW and the cassette is 445 °C, 354 °C and 286.3 °C respectively. After the failure, the maximum temperature on each component is almost unaltered.

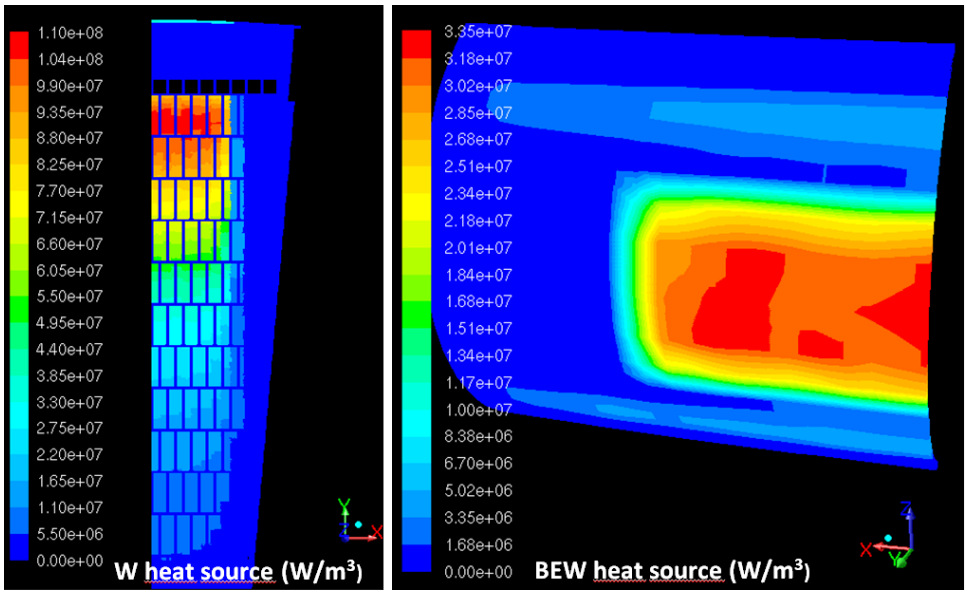

Figure 75: Thermal source at average current generated in the spallation material an the PBEW by the raster focused beam

Figure 76 shows the maximum temperature of the different areas of the target vessel when steady state is achieved. There are no significant changes on temperature profiles.

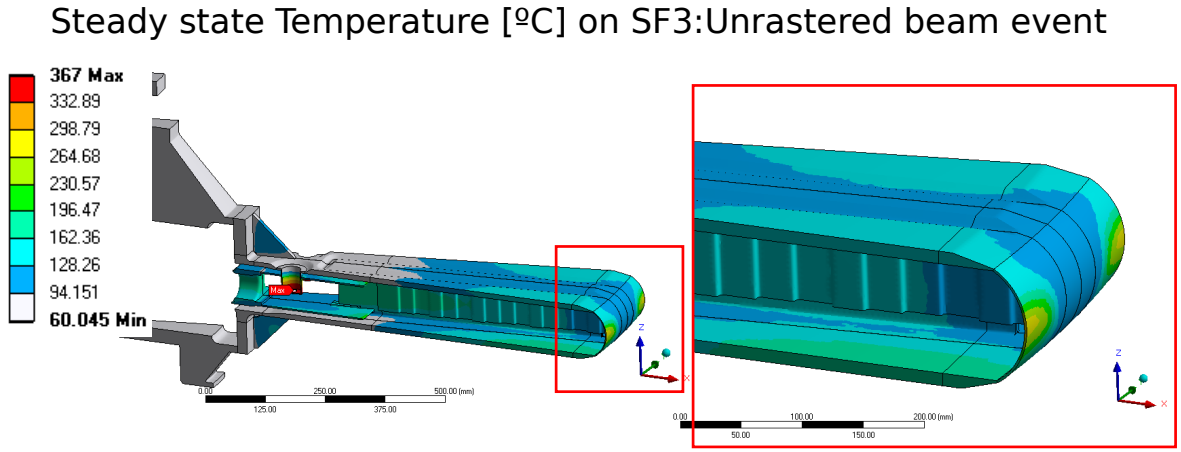

Figure 76: Temperature distribution for rastered-focused beam event.

Regarding secondary loads mechanical stresses, Figure 77 shows the equivalent stress distribution. Consequently with the temperature distribution showed on previous section, there is no significant changes in the secondary loads stress distribution. The linearized analysis in the PBEW shows that most of the stress is mainly $P_m + Q_m$ and it achieves 280 MPa however, which is a factor of 10 below the S^A_{em} limit at 3.75 dpa and 300^oC ($\sim$ 2827 MPa).

According to temperature and stress distributions, the target can operate under raster focused beam under protection level A.

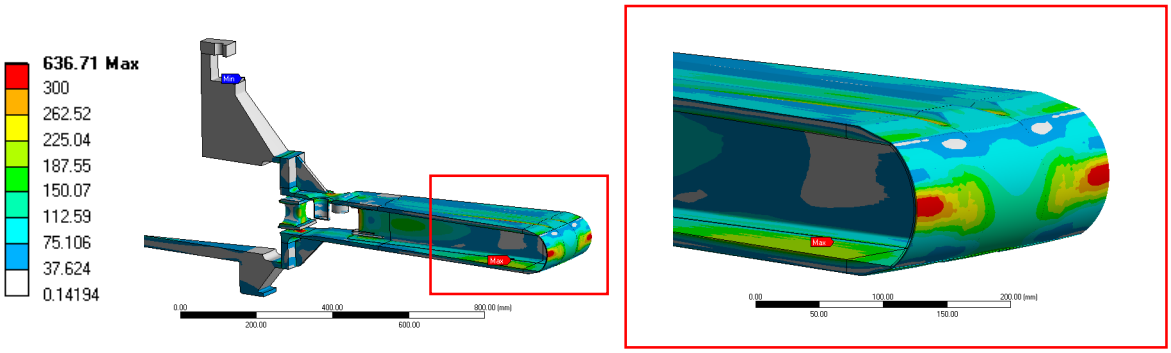

Figure 77: Von Misses equivalent stress for steady state conditions on rastered-focused beam.

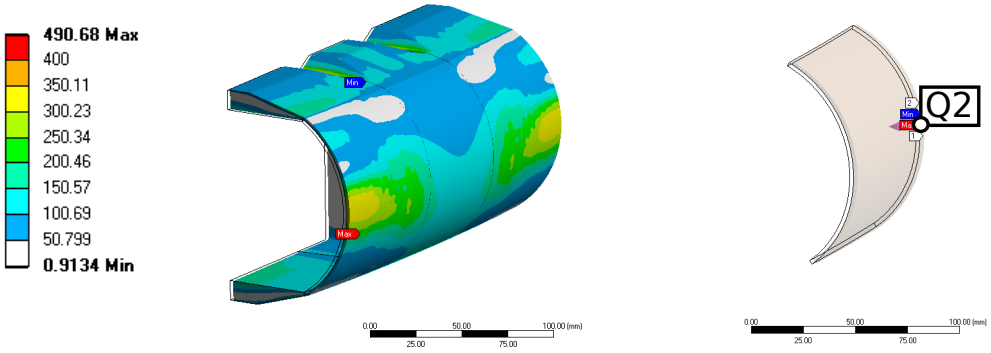

Figure 78: PBEW Von Misses equivalent stress for steady state conditions on rastered-focused beam.

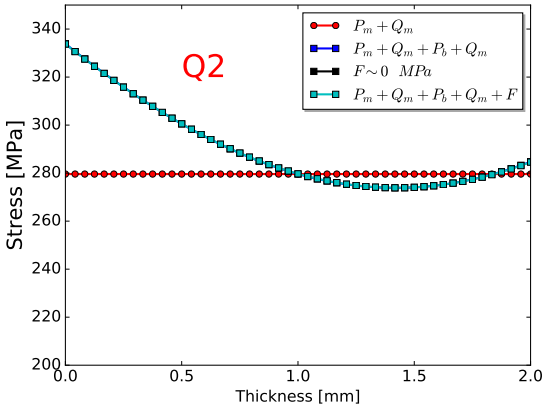

Figure 79: PBEW linearized equivalent Von Misses analysis on path Q2 showed on Figure 78.

8.9 SF4: Stopped Wheel

The Stopped wheel event is reproduced when the wheel stops and the proton beam continue heating the target. In this conditions, the sector in front of the beam will increase its temperature almost adiabatically because the time in between pulses ($\sim$ 68 ms) is not enough to remove a significant amount of heat with the helium flow.

In order to reproduce this accident, two scenarios has been evaluated based on the FEM model 5.5. In the first scenario, heat transfer coefficients has been removed form the analysis with correspond with the adiabatic increase of temperature (conservative scenario). In the second one, heat transfer coefficients evaluated on CFD analysis for nominal conditions are maintain, including the temperature of the helium with is not realistic. This second scenario will provide optimistic conditions from heat removal. In both cases, the heat deposition in the BEW is time average.

Figure 80 shows the maximum temperature of the wheel and the BEW in both scenarios. There is no significant differences in the behavior of the BEW which confirms tha the process can be consider adivatic with low error.

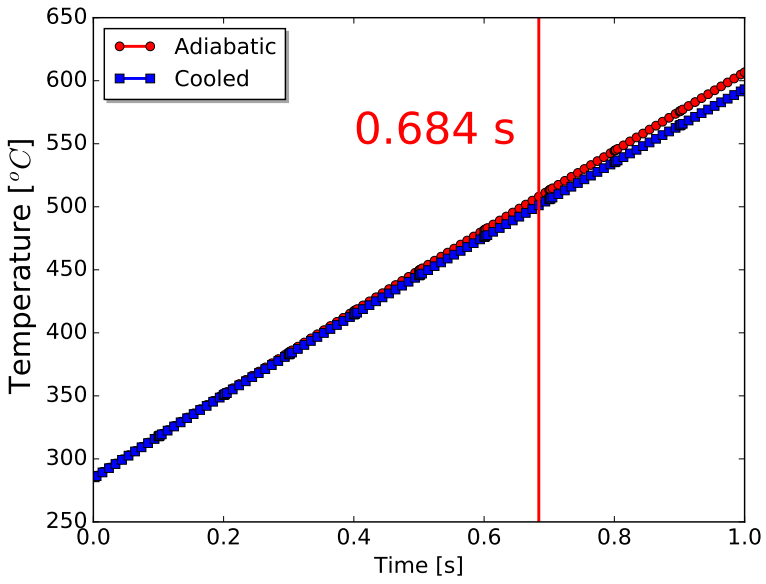

Figure 80: Temperature distribution on the PBEW for wheel block.

Figure 81 shows the temperature distribution after 0.68 s when the 500^oC is achieved. On this time step the stress distribution of the vessel (Figure 82) shows still values below S^A_{em} (S^A_{em} = 1134 MPa, for 3.75 dpa and 500^oC). According to this values, the stress distribution

is below the protection level A, consequently the limit for the accident is defined by the temperature. The temperature of 500^oC will be achieved after 10-11 pulses of the beam that is considered the operational limit of vessel the material.

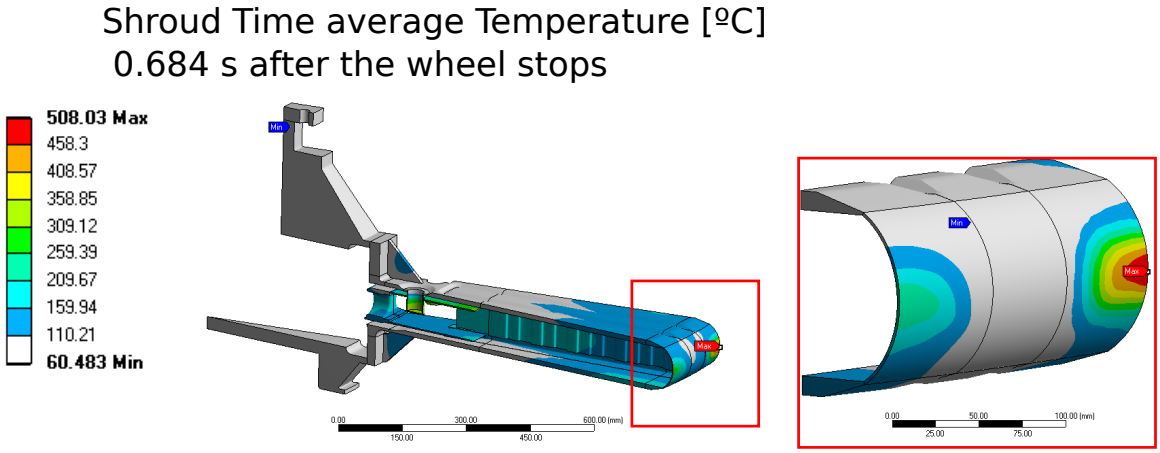

Figure 81: Temperature distribution on the Target wheel after 0.68 s for wheel stop accident.

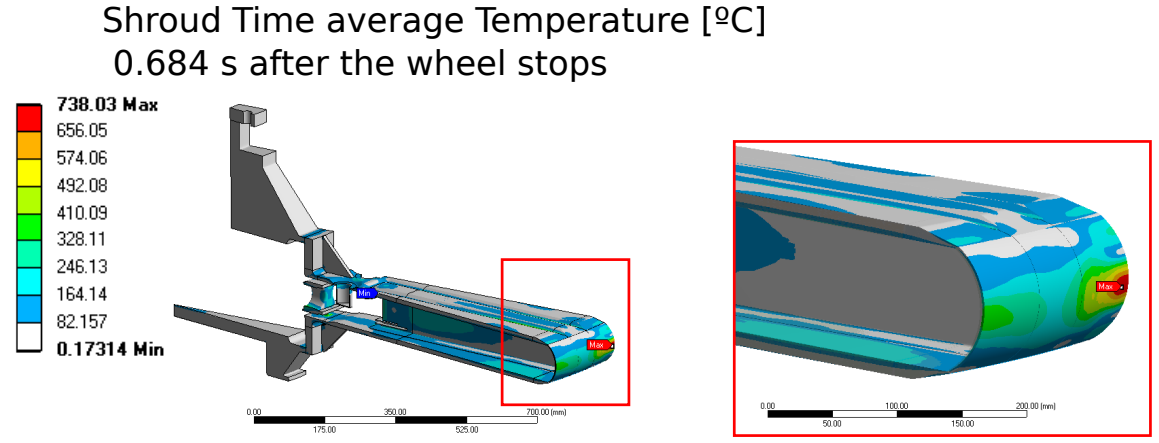

Figure 82: Equivalent Von Misses stress distribution on the Target wheel after 0.68 s for wheel stop accident.

8.10 SF4: Unrastered-overfocused beam

The unraster-focused beam is an extreme event produced when double failure is produced. This conditions produced a 15 mm beam on the target. The pulse length is 2.85 ms hence, heat transfer during the pulse is not significant and the problem can be considered as an adiabatic increase of temperature in the footprint of the beam. However, the beam relative small and the rotating of the wheel will increase significantly the affected area. Figure 83 shows and scheme of the affected are in the accident.

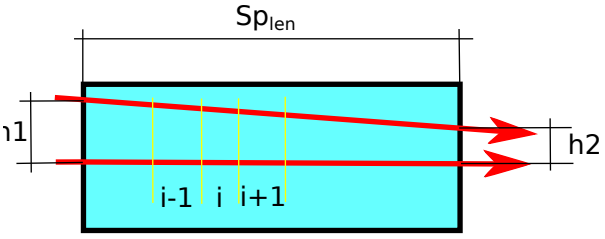

Figure 83: Thermal affected volume

The values H1 and H2 are proportional to the angular velocity of the target, radius and pulse length. The ratio between the thermal affected are and the footprint gives the dilution factor to the heat load. Due to the geometrical dilution effect associated with the radius, the dilution is higher in the external radius that math with the higher heat load.

$$H1 = \omega \cdot R1 \cdot T_{pulse} \tag{1}$$

$$H2 = \omega \cdot R2 \cdot T_{pulse} \tag{2}$$

$$Footprint = \pi \cdot \phi^2 SP_{len} \tag{3}$$

$$Dilution = \frac{Footprint}{Foorprint + \phi \cdot SP_{len} \cdot (H1 + H1)/2} \tag{4}$$

Figure 84 shows the heat load profile associated with the dilution factor along the spallation material radius.

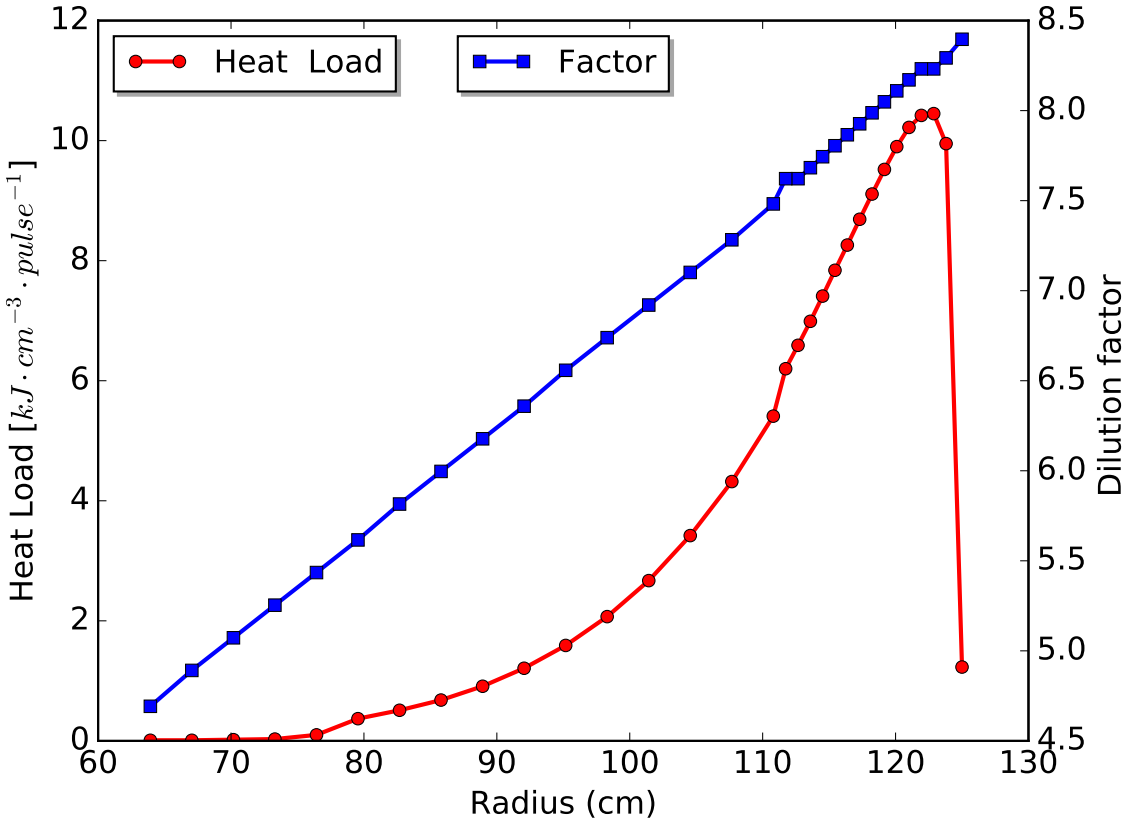

Figure 84: Heat load and dilution factor along the radius

The analysis is performed assuming that the heat conduction is not significant during the pulse length hence ,and adiabatic increase of temperature is produced. The increase of temperature up to the melting point can be evaluated by the following expression:

$$\Delta T_i = \frac{q_i''' \cdot v_i}{\rho \cdot C_p v_i \cdot Dilution_i} \tag{5}$$

Where q_i''' is the heat load in the volume of the volume of the footprint (v_i). From the release point of view a conservative approach is to considered that we release all the activated inventory in the melting point of the tungsten. The second conservative approach is assume that when the material is melt is is removed from the position and the remaining heat will be transfer to next element in the beam direction. The following expression describes the increase of temperature

in the element $i+1$ when the heat load in the element i is enough to increase the temperature above the melting point:

$$\Delta T_{i+1} = \frac{q'''_{i+1} \cdot v_{i+1} + (q'''_i \cdot v_i - \rho \cdot C_p \cdot v_i \cdot (T_{melting} - T_i) - Q_{melting} \cdot v_i)}{\rho \cdot C_p v_i \cdot Dilution_i} \quad (6)$$

This analysis maximized the amount of material that can be melt. Figure 85 shows the temperature distribution along the W radious. Hence, there is not enought energy to cross the spallation material in a single shot.

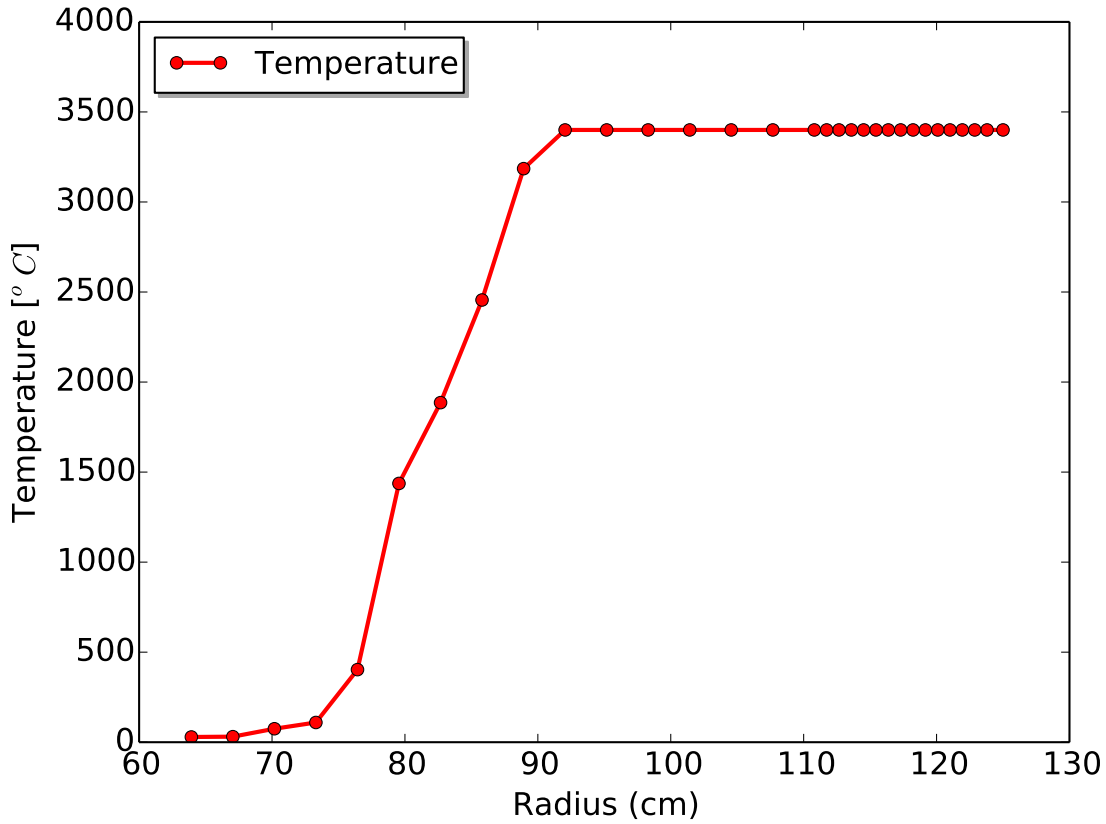

Figure 85: Temperature distribution along the spallation material radius. Adiabatic increase of temperature and melting

If we consider the BEW, the heat load in the material will be in the range of $\sim 4.2 KJcm^{-3} pulse^{-1}$. According previous analysis, the increase of temperature in a single shot will be:

$$\Delta T_i = \frac{q_i'''}{\rho \cdot C_p \cdot Dilution_i} = \frac{4.2[kJcm^{-3}pulsem{-}1]}{0.504[kJkg^{-1}K^{-1}] \cdot 8.5} > 1400^oC \quad (7)$$

Therefore, the BEW will not survive to this event and the pressure barrier will be broken.

9 Conclusions

The previous sections shows the load cases analyzed for Target Vessel for the ESS Target. The following conclusions can be remarked:

- SF1- Design conditions: The proposed configuration fulfill the $RCC - MR_x$ requirements for protection level A.
- SF1- Nominal conditions: The proposed configuration fulfill the $RCC - MR_x$ requirements for protection level A.
- SF2- Wheel-beam desynchronization: The Target wheel failure will be produced after 14 pulses.
- SF2- Shutdown: Maximum temperature of the Target shroud will be below the design conditions.
- SF2- Lost of cooling: Based on maximum temperature of the shroud, the Target Vessel will be below design conditions up to 70% of mass flow reduction.
- SF3- Rastered-focused beam: The proposed configuration fulfill the $RCC - MR_x$ requirements for protection level A.
- SF3- Unrastered-nominal beam: The proposed configuration fulfill the $RCC - MR_x$ requirements for protection level A in the vessel.
- SF4- Stopped Wheel: The proposed configuration fulfill the $RCC - MR_x$ requirements for protection level A in the vessel.
- SF4- Unrastered-overfocused beam: The BEW will not survive to this event and the pressure barrier will be broken in a single pulse. However, the total of W released is relative small.

In summary, all the proposed scenarios for Target Wheel operation has been analyzed according to $RCC - MR_x$ $N2R_x$ requirements. Based on that, the target wheel can be consider acceptable from thermomechancial point of view.

References

[1] ESS-0060792: WP2 Target wheel, drive and shaft design basis for pressure- and load retaining components

[2] Reference is needed.

[3] Lebarbe, T., et al. "Presentation of the Afcen RCC-MRx Code for Sodium Reactors (SFR), Research Reactors (RR) and Fusion (ITER): General Overview." ASME 2010 Pressure Vessels and Piping Division/K-PVP Conference. American Society of Mechanical Engineers, 2010.

[4] ESS-0037038: Load Cases, Classification and system parts Target Wheel, Drive and Shaft

[5] ESS-0003310: Beam on Target Requirements

[6] ESS-0131487: Target Vessel Manufacturing Specification

[7] ESS-0086974: Measurement system configuration for target sectors miss-balance fow evaluation

[8] ESS-0066301: Target, Shaft and Rotating seal CFD model

[9] ESS Target Materials Handbook (ESS-0028465)

[10] Andersen, K. "ESS Technical Design Report." (2012).

[11] ESS-0036673: ESS-Bilbao Target Proposal

[12] F.J. Alonso, J. Sanz, J.M. Perlado, Daño en materiales estructurales candidatos para un reactor comercial de fusión, DENIM 198, 1989

[13] ESS-0055645: Vibration test

[14] Dai, Y., et al. "The second SINQ target irradiation program, STIP-II." Journal of nuclear materials 343.1 (2005): 33-44.

[15] SuperMC/MCAM 5.2 User Manual, Institute of Nuclear Energy Safety Technology, CAS

[16] ESS-0051512: Neutron Activation Analysis ESS

[17] Sanz, J., O. Cabellos, and N. García-Herranz. "ACAB-2008, ACtivation ABacus Code V2008." NEA Data Bank NEA-1839 (2008).

[18] Goorley, T., et al. "Initial MCNP6 release overview." Nuclear Technology 180.3 (2012): 298-315.

[19] ESS-0037287: Radiation Damage Analysis for the ESS Target

[20] K. K. Gudima M. I. Baznat et al CEM03.S1, CEM03.G1, LAQGSM03.S1, and LAQGSM03.G1 Versions of CEM03.01 and LAQGSM03.01 Event-Generators. Technical report, Los Alamos National Laboratory, March 2006

[21] MCNPX user's Manual. Version 2.6.0. 2007

[22] Konobeyev, A. Yu, and U. Fischer. "Evaluation of displacement and gas production cross-sections for structure materials using advanced simulation methods and experimental data." INDC (NDS)-0648 (2013): 22.

[23] ESS-0058358: Equipment specification document: Spallation Material

[24] ESS-0030245: ICD-R: Casks and Associated Handling Devices Target Systems

[25] Clarifications and answers to CDR Spallation Material

[26] Section III - Tome 1 - Subsection Z - Appendix A3.3S: PropertiesGroups for products and parts in X2CrNiMo17-12-2, X2-CrNiMo17-12-3, X2CrNiMo18-14-3 solution annealed austenitic stainless steels

[27] ESS-0235921: Emissivity report

[28] ESS-0012896: ESS Vacuum Handbook Part 3 - ESS Vacuum Design & Fabrication

[29] ESS-0034495 Design beam footprints for the Target- Accelerator interface

[30] Fatigue assessment of the Target Wheel.

[31] ESS-0219229: Target Shaft manufacturing and inspection plan

[32] ESS-0145049: Target wheel inspection plan

[33] ESS-0237938: Detail Residual heat load calculations

[34] ESS-0131487: Target Vessel Manufacturing Plan and inspection plan